HHS Public Access

Author manuscript

Nat Chem Biol. Author manuscript; available in PMC 2023 July 10.

Published in final edited form as:

Nat Chem Biol. 2023 July ; 19(7): 815–824. doi:10.1038/s41589-023-01273-x.

Depletion of creatine phosphagen energetics with a covalent creatine kinase inhibitor

Narek Darabedian[1,2,*], **Wenzhi Ji**[3,*], **Mengyang Fan**[3], **Shan Lin**[4], **Hyuk-Soo Seo**[1,5], **Ekaterina V. Vinogradova**[6], **Tomer M. Yaron**[7,8,9,10,11], **Evanna L. Mills**[1,2], **Haopeng Xiao**[1,2], **Kristine Senkane**[12], **Emily M. Huntsman**[7,8], **Jared L. Johnson**[7,8], **Jianwei Che**[1], **Lewis C. Cantley**[1,2], **Benjamin F. Cravatt**[12], **Sirano Dhe-Paganon**[1,5], **Kimberly Stegmaier**[4], **Tinghu Zhang**[3], **Nathanael S. Gray**[3,#], **Edward T. Chouchani**[1,2,#]

[1]Department of Cancer Biology, Dana–Farber Cancer Institute, Boston, MA, USA.

[2]Department of Cell Biology, Harvard Medical School, Boston, MA, USA.

[3]Department of Chemical and Systems Biology, CHEM-H and SCI, Stanford Medical School, Stanford University, Stanford, CA, USA.

[4]Department of Pediatric Oncology, Dana-Farber Cancer Institute, Boston, MA, USA.

[5]Department of Systems Biology, Harvard Medical School, Boston, MA, USA.

[6]Laboratory of Chemical Immunology and Proteomics, The Rockefeller University, New York, NY, USA.

[7]Meyer Cancer Center, Weill Cornell Medicine, New York, NY, USA.

[8]Department of Medicine, Weill Cornell Medicine, New York, NY, USA.

[9]Englander Institute for Precision Medicine, Institute for Computational Biomedicine, Weill Cornell Medicine, New York, NY, USA.

[10]Department of Physiology and Biophysics, Weill Cornell Medicine, New York, NY, USA.

[11]Tri-Institutional PhD Program in Computational Biology & Medicine, Weill Cornell Medicine/ Memorial Sloan Kettering Cancer Center/The Rockefeller University, New York, NY, USA.

[#]Corresponding author: nsgray@stanford.edu, edwardt_chouchani@dfci.harvard.edu.
[*]These authors contributed equally

Author Contributions: E.T.C. and N.S.G. conceived of and designed the study. N.D. and S.L. performed cellular experiments and analyzed data. W.J., M.F., J.C., and T.Z., designed and conducted chemical syntheses. N.D. E.M.H, J.L.J, and T.M.Y carried out and analyzed data from mass spectrometry experiments. N.D. assisted with protein expression and purification. H.X. developed the CPT screening platform. E.V.V., K.S. and B.F.C. conceived, designed, and conducted gel-based screening experiments. E.L.M. performed macrophage experiments and metabolomics experiments. S.D. oversaw CK expression and purification and crystallization. J.C. performed molecular modeling. K.St. and S.L. contributed to conceptual design and provided cellular reagents. E.T.C. and N.S.G. directed research, oversaw the experiments, and wrote the manuscript with assistance from the other authors.

Competing financial interests: N.S.G. is a founder, science advisory board member (SAB) and equity holder in Syros, C4, Allorion, Jengu, B2S, Inception, Matchpoint, CobroVentures, GSK, Larkspur (board member) and Soltego (board member). The Gray lab receives or has received research funding from Novartis, Takeda, Astellas, Taiho, Jansen, Kinogen, Arbella, Deerfield, Springworks, Interline and Sanofi. E.T.C is a founder, board member and equity holder in Matchpoint Therapeutics and Aevum Therapeutics. T. Z. and J.C. are founders, equity holders and consultants in Matchpoint Therapeutics. J.C. is a scientific co-founder M3 Bioinformatics & Technology Inc., and consultant and equity holder for Soltego and Allorion. K.St. has funding from Novartis Institute of Biomedical Research and Kronos Bio, consults for and has stock options in Auron Therapeutics and previously consulted for Kronos Bio and AstraZeneca. T.M.Y. is a co-founder, stockholder and on the board of directors of DESTROKE, Inc. T. Z. W.J. N.D. N.S.G. and E T.C. are inventors on a patent for CK inhibitors WO 2022/087433 A8. All other authors declare no potential conflict of interest.

[12]Department of Chemistry, The Scripps Research Institute, La Jolla, CA, USA.

Abstract

Creatine kinases (CK) provide local ATP production in periods of elevated energetic demand, such as during rapid anabolism and growth. Thus, creatine energetics has emerged as a major metabolic liability in many rapidly proliferating cancers. Whether CKs can be targeted therapeutically is unknown, as no potent or selective CK inhibitors have been developed. Here we leverage an active site cysteine present in all CK isoforms to develop a selective covalent inhibitor of creatine phosphagen energetics, CKi. Using deep chemoproteomics, we discover that CKi selectively engages the active site cysteine of CKs in cells. A co-crystal structure of CKi with creatine kinase B (CKB) indicates active site inhibition that prevents bi-directional phosphotransfer. In cells, CKi and its analogues rapidly and selectively deplete creatine phosphate, and drive toxicity selectively in CK-dependent AML. Finally, we use CKi to uncover an essential role for CKs in regulation of pro-inflammatory cytokine production in macrophages.

Introduction

The reversible transfer of a phosphoryl group between ATP and creatine is central to cellular bioenergetics. This reaction is facilitated by four creatine kinases (CK) that are differentially localized within the cell. Two mitochondrial isoforms of CK, CKMT1 (creatine kinase ubiquitous-type, mitochondrial) and CKMT2 (creatine kinase sarcomeric-type, mitochondrial), are proximal to the major site of ATP production in the cell. In addition, there are two cytosolic isoforms, CKM (creatine kinase, muscle-type) and CKB (creatine kinase, brain-type). This distinct localization allows CKMTs to generate phosphocreatine from mitochondrial ATP, and cytosolic CKs to rapidly replenish ATP throughout the cell in periods of high ATP demand[1].

Genetic loss of function studies have shown that loss of the CK circuit has modest effects on the basal energetics of cells and tissues, but significantly affects cellular processes that rely on high ATP demand[1]. As such, CKs appear to be primarily relevant for buffering ATP-dependent processes in periods of rapid ATP utilization. Numerous cancers have co-opted creatine phosphagen energetics to facilitate rapid growth and survival, and CKs are a major metabolic liability in metastatic disease. CKs are essential for growth and metastasis of aggressive acute myeloid leukemias (AML)[2], liver and breast cancer metastases[3–5], and pancreatic cancers[6]. Importantly, the essentiality of CKs for these cancers is distinct, as somatic tissues do not rely on CKs for viability suggesting an ample therapeutic index for this target[7–10].

Acute myeloid leukemia (AML) is a prominent example of creatine-reliant cancer, which is associated with poor clinical outcomes and relies critically on CK-mediated generation of phosphocreatine[2]. While the metabolic liability of CKs in cancers is clear based on genetic evidence, pharmacologic targeting of creatine energetics has proven a challenge. Inhibition of creatine utilization in cells has been limited to the use of non-metabolized creatine analogues that compete for creatine binding with creatine transporters[11,12]. While these studies demonstrate the therapeutic promise of inhibiting creatine energetics generally,

the non-specific nature and low potency of these tools limits their therapeutic utility. More generally, the relevance of CKs in other cellular processes has been stifled by the lack of specific tools for efficient inhibition of the four CK isoforms. Because of the need for technologies to selectively inhibit CK energetics, and to explore the therapeutic potential of inhibiting CKs in cancer, herein we develop a potent and selective inhibitor of CKs. We leverage an active site cysteine present in all CK isoforms to develop a selective covalent inhibitor of creatine phosphagen energetics, CKi.

Results

Deep chemoproteomics identifies CKi.

CKs possess a highly conserved active site that contains a cysteine residue essential for activity (Figure 1a)[13–16]. We noted that this cysteine is subject to endogenous post-translational oxidative modification across all isoforms[17], suggesting that the constituent thiolate has a high nucleophilicity (Figure 1b). On this basis, we hypothesized that the CK active site cysteine (Cys283 using CKB and CKM numbering) may be amenable to selective targeting by a small molecule containing an appropriately oriented electrophilic warhead. It is now well appreciated that solvent accessible, nucleophilic cysteine thiolates can be selectively targeted by small molecule electrophiles[18], and ligandability datasets have suggested that CK cysteines may be amenable to such an approach[19,20]. Moreover, with the advent of quantitative cysteine chemoproteomics methods, it is now possible to query protein cysteines under native conditions for engagement with cysteine-reactive small molecules[19–22]. An additional advantage of chemoproteomic assessment of cysteine electrophiles is that quantitative engagement with thousands of cysteines is provided, allowing for an estimation of the selectivity of the small molecule in question.

Current chemoproteomic workflows quantify engagement of molecules with ~5,000–15,000 cysteines in a single experiment. We reasoned that improved coverage of the cysteine proteome would allow for robust identification of a selective and potent CK active site cysteine labeler. We had recently developed a cysteine labeling and enrichment reagent for quantitative proteomics, called cysteine-reactive phosphate tags (CPT) [17]. CPTs facilitate >99% enrichment of cysteine-containing peptides using metal affinity chromatography (IMAC) enrichment, allowing for deep mapping of the cysteine proteome[17]. We posited that CPTs could be deployed in a chemoproteomics workflow for deep mapping of the cysteine proteome to assess quantitative engagement of cysteine-reactive small molecules simultaneously with tens of thousands of cysteines (Figure 1c). We found that combining CPT with tandem mass tag (TMT)-multiplexed chemoproteomics, we could quantify small molecule engagement with ~23,000–32,000 cysteines in a single experiment, and over 40,000 cysteines across replicate experiments (Supplementary Table 1).

Using CPT-MS we screened intact human AML cells (UCSD-AML1) for small molecules that could potently and selectively engage the CK active site cysteine. To do so, we used commercially available cysteine-focused library from Enamine comprising fragments containing chloroacetamide warheads. Querying a subset of this library for reactivity with recombinant CKB identified fragments that exhibited engagement (Extended Data Fig. 1a,b & Supplementary Table 2). Of those molecules that exhibited engagement with CKB, one

did so absent non-specific reduction in signal that is indicative of promiscuous labeling. This molecule, henceforth referred to as CKi **(CKi-1)**, was prioritized for screening in intact UCSD-AML1 cells. UCSD-AML1 were employed because they express high levels of CKMT1 and CKB, and creatine energetics are an established metabolic vulnerability in these cells[2]. From this initial analysis CPT-MS identified that CKi covalently modified the active site cysteine of both CKMT1 and CKB, the two CK isoforms expressed in UCSD-AML1 (Figure 1d). CKi exhibited a very high degree of proteome-wide selectivity for the CK active site cysteine at low μM concentrations. Between 5–20 μM, CKi reproducibly and selectively labelled the CKMT1 and CKB active site cysteines (Figure 1e & Supplementary Table 3). At these concentrations, CKi labelled 4–18 cysteine sites over 50% stoichiometry, corresponding to CK off-target engagement of 0.017–0.078% of the observable cysteine proteome (Figure 1d,e). Only two non-CK cysteines were consistently engaged proteome wide by CKi, on two glutathione S-transferase proteins GSTO1 and GSTCD (Figure 1e and Supplementary Table 3), which are proteins known to engage with a range of small molecule electrophiles[23]. CKi engagement of the CKMT1 and CKB active site cysteine in intact cells was concentration dependent and readily achieved at 1 μM (Figure 1f). We confirmed direct labeling of CKs by CKi by examining the intact mass of recombinant human CKB. Incubation of CKB with CKi resulted in a mass shift of the protein corresponding to the mass of a CKi adduct (Figure 1g). Peptide analysis of recombinant CKB determined that this labeling was attributable to covalent modification of the active site Cys283 (Figure 1h). We additionally confirmed labeling of CKB by CKi in intact cells by generating a CKi analogue amenable to biotin conjugation, which we established could also label CKB (Extended Data Fig. 1c,d). UCSD-AML1 cells were treated with CKi-alkyne **(CKi-2)**, lysed, and were incubated with biotin-azide followed by avidin enrichment, which demonstrated robust enrichment for CKB at as low as 310 nM **CKi-2** (Figure 1i & Supplementary Information). Conversely, pre-treatment of cells with CKi followed by a molar excess of **CKi-2** demonstrated that biotin enrichment of CKB could be fully competed by CKi (Figure 1j). **CKi-2** treatment of cells followed by conjugation with a fluorophore indicated that this molecule confirmed proteome-wide selectivity (Extended Data Fig. 1e). We also determined the capacity for CKi to label other CKs by examining cell types that express each of the four isoforms, finding that **CKi-2** could label them all (Figure 1k). Taken together, these data uncover CKi as a potent and selective electrophile targeting the active site cysteine of CKs *in vitro* and in cells.

Structural basis for CKi-mediated inhibition of CKs.

To evaluate the binding mode of CKi, we determined the co-crystal structure of CKB in complex with CKi at 2.93Å resolution (Supplementary Table 4). CKi bound partially in the ATP and creatine-binding pockets composed of helices α3 and α8 and loops α3/4 and α9-ß6 (Extended Data Fig. 1f). The structure showed clear electron density to Cys283 in the 2FO-FC electron density map, which confirmed a covalent interaction (Figure 2a). The amide group of CKi mediated hydrogen bonds to the backbone nitrogen of Gly-73, the hydroxyl side chains of Thr-71 and Thr-59; the latter was also hydrogen bonded with the oxygen of the dihydro-oxazine (Figure 2a & Extended Data Fig. 2a). The phenyl of the bicyclic rings of CKi covered a shallow hydrophobic patch of comprised of Val-75, Met-207, and Leu-202, with the dihydro-oaxizine of the bicyclic rings as well as the amide

carbonyl oxygen of the electrophilic group mostly solvent exposed, suggesting opportunities for further modification and chemical optimization of CKi.

CK catalysis involves open and closed conformations, with substrate and cofactor binding inducing clamping or closure of the ß7/8 and α3/4 loops[24]. In our structure, the conformation of the CKi complex corresponded to the open form with minimal alterations of residue packings around the creatine binding site and no apparent alterations in homodimer packing and cooperativity (Figure 2b). By directly and sterically competing with creatine, CKi is predicted to block catalytic turnover, preventing formation of the ATP/creatine ternary complex.

The binding mode of CKi suggests that it would effectively inhibit CK phosphotransfer activity. We examined recombinant CKB activity and found that CKi inhibited creatine phosphate generation, exhibiting an apparent IC_{50} of 1.2 μM (Figure 2c). We examined kinetics of inhibition and engagement of CKB by CKi, observing time and concentration dependence, and maximal inhibition at a given concentration was achieved by 2h (Extended Data Fig. 2b,c). We assessed the kinetic efficiency of the CKi reaction with CKB by determining the second order rate constant k_{inact}/K_I to be ~0.189 $\mu M^{-1}min^{-1}$ (Extended Data Fig. 2d). CKi inhibition occurred in the presence of thiol reducing agents, and a CKi analogue lacking the chloroacetamide warhead (**CKi-3**) abrogated inhibition (Figure 2d). Using the CKi-CKB co-crystal as a guide, we next explored the tolerability of the CKi scaffold **(CKi-4 to CKi-23)** to modification (Figure 2e and Supplementary Table 5). The co-crystal structure of CKi with CKB reveals that the hydrophobic pocket is not fully occupied by the CKi phenyl group. Therefore, we introduced additional lipophilic groups to the phenyl component of CKi. While most of these groups do not lead to an improvement on CKB inhibition, bromo and phenyl groups indeed showed superiority to hydrogen and offered 2–4 fold improvement on biochemical IC_{50}s. In addition, methylation of amide group was tolerated and showed a comparable IC_{50} to CKi. As for the cysteine covalent warhead, while electrophiles with tempered reactivity towards cysteine, such as acrylamide, have been used in many cysteine targeting covalent molecules, our efforts of switching chloroacetamide to either acrylamide or sulfonamide were not fruitful, indicating the possibility of spatial restriction on the reaction coordinates. Finally, we synthesized enantiomerically pure forms of CKi (Figure 2f), which revealed that the *S*-enantiomer (*S*-CKi, **CKi-24**) exhibited elevated potency compared to the racemic mixture (Figure 2f). Conversely, *R*-CKi (**CKi-25**) exhibited an order of magnitude decrease in potency (Figure 2f). Additional analogues representing the breadth of observed inhibitory activity are provided in the SI (Supplementary Table 5).

CKi and MitoCKi deplete cellular phosphocreatine.

We next examined the cellular consequences of CK inhibition by CKi. We treated UCSD-AML1 cells with 20 μM CKi and monitored the levels of major cellular metabolites, including creatine and phosphocreatine. By 16 hr following treatment with CKi, we observed a highly selective reduction in cellular phosphocreatine (Figure 3a & Supplementary Table 6). Titrating CKi, we observed significant depletion of phosphocreatine at 1 μM, and maximal inhibition at 10 μM (Figure 3b). Upon maximal

depletion of phosphocreatine, cellular ATP/ADP decreased dramatically (Extended Data Fig. 2e), as did the abundance of guanine and adenine nucleotides overall (Supplementary Table 6). Depletion of these species coincided with accumulation of guanine and adenine (Supplementary Table 6), supporting the notion that creatine energetics is key for supporting purine nucleotide anabolic pathways in UCSD-AML1 cells. Significant depletion of phosphocreatine was observed by 1 hr (Figure 3c). Interestingly, creatine levels were marginally increased by CKi only at some concentrations of CKi (Figure 3b,c), which is perhaps a consequence of continued creatine production and utilization by metabolic pathways independent from the creatine phosphagen system. Highly selective depletion of phosphocreatine was indicative of inhibition of the CKMT-mediated reaction to generate cellular phosphocreatine.

To improve cellular potency of CKi, we considered the fact that CKMTs are mitochondrially localized. Since CKMTs mediate the proximal phosphotransfer reaction in the CK circuit to generate phosphocreatine, improved targeting of the mitochondrial isoforms specifically should improve potency for depletion of cellular phosphocreatine. In light of this, we explored whether inclusion of a triphenylphosphonium(TPP)-conjugated analog of CKi could improve cellular activity (Figure 3d). Based on the delocalized positive charge of TPP, it concentrates substantially in the cytosol, and even more so in the mitochondrial matrix due to the distinct net negative charge of this sub-cellular compartment, and rapid exchange of TPP across lipid bilayers[25]. We reasoned that CKMTs, which are localized in the mitochondrial intermembrane space, could therefore be more readily engaged by a TPP-conjugated CKi derivative. Based on this hypothesis, we generated MitoCKi **(CKi-26)**, whereby CKi was conjugated to alkyl-TPP at a scaffold position permissive to modification (Figure 3d). We examined recombinant CKB activity and found that MitoCKi inhibited creatine phosphate generation, exhibiting an IC_{50} of 185 nM (Figure 3e). The increase in biochemical potency of MitoCKi might be due to hydrophobic interaction of the tail with the protein flexible loops next to the binding site. To examine this possibility, we synthesized CKi derivatives with varying alkyl chains in place of alkyl-TPP **(CKi-27 to CKi-29)** and found that above four carbons, alkyl chain improved biochemical potency (Extended Data Fig. 2f,g). Titrating MitoCKi in cells, we observed significantly improved efficacy in depletion of cellular phosphocreatine, with over 50% depletion observed at 1 μM (Figure 3f). Again, these effects occurred rapidly, with significant depletion observed by 1 h (Figure 3g).

CKi and MitoCKi are cytotoxic to CK-dependent AML.

CKs are essential for viability of AMLs[2], so here we examined the consequences of CKi and MitoCKi in this context. Both CKi and MitoCKi arrested growth and induced cytotoxicity in UCSD-AML1 cells, an EVI1-positive AML that is particularly reliant on CKMT1 for viability (Figure 4a,b). The EC_{50} for both CKi and MitoCKi matched closely with the effective concentrations for depletion of phosphocreatine (Figure 3b,f). Moreover, cytotoxicity against a panel of patient-derived AMLs was comparable to UCSD-AML1 (Figure 4c). We next sought to better understand whether inhibition of CKs by CKi's explained toxicity in AML. Since the CK active site cysteine is essential for phosphotransfer activity, a cysteine loss of function mutant would not be informative for this question.

Instead, we examined CKi analogs for the relationship between capacity for CK inhibition *in vitro*, and cellular toxicity in UCSD-AML1. Modification of select regions of the CKi scaffold tuned CK cytotoxic potency, which correlated well with CK inhibitory efficacy (R^2=0.85), providing evidence for on-target toxicity (Figure 4d). Interestingly, cytotoxic concentrations of CKi and MitoCKi in cancer cells that do not rely genetically on CK for viability were significantly higher (Figure 4e,f). To investigate this further, we compared the effects of CKi on phosphocreatine levels in UCSD-AML1 and A549, an exemplar non-CK sensitive cell type[26]. While CKi rapidly depleted phosphocreatine in UCSD-AML1 cells, it had no effect on phosphocreatine in A549s (Extended Data Fig. 2h), supporting the conclusion that CKi is selectively toxic to cells that rely on phosphocreatine utilization to support growth and proliferation. Finally, we predicted that if CKi was cytotoxic through inhibition of CKs, then increasing the pool of CKs in a CK-dependent cell type would increase the EC_{50} of CKi. We attempted to over-express the two major CK isoforms expressed in multiple CK-reliant cell types but most were recalcitrant to forced over-expression, likely due to high basal levels of CK. Nonetheless, we were able to generate HEK293 cells with about 2-fold elevated CKB content (Extended Data Fig. 2i) over baseline, HEK293s being another known CK-reliant tumorigenic cell line[26] with similar sensitivity to CKi as AMLs (Extended Data Fig. 3a). Interestingly, doubling of CKB content in HEK293 cells more than doubled the EC_{50} of CKi (Extended Data Fig. 3a). Together, these data provide further evidence of toxicity of this series being mediated primarily through depletion of creatine energetics.

Previous work has shown that CK-dependent AMLs are unusually reliant on creatine phosphagen energetics to support cellular growth and division[2]. We therefore examined whether cytotoxicity initiated by CKi series modulated these processes selectively in CK-dependent AML. We first applied phosphoproteomics to better understand the acute signaling response to CKi and MitoCKi, which would provide a basis for understanding its selective cytotoxicity in AML. We applied minimal effective concentrations of both molecules in UCSD-AML1 cells and a non-CKi sensitive A549 cell line[26] for 16 h, followed by MS analysis. Phosphoproteomic data was processed to determine kinase cascades that were induced by both CKi and MitoCKi selectively in UCSD-AML1 (Extended Data Fig. 3b,c & Supplementary Table 7). To determine this, we used a newly developed algorithm that systematically classifies differentially regulated phosphorylation sites based on the kinases that target these residues (Extended Data Fig. 3c & Supplementary Table 7 & Methods for details).

This analysis found that CKi and MitoCKi initiate kinase signaling cascades that are hallmarks of the DNA damage response, as well as cell cycle kinases, selectively in UCSD-AML1 cells (Extended Data Fig. 3c–e). Specifically, we observed robust elevation in ATM, ATR, DNAPK, and SMG1 phosphorylation signatures (Extended Data Fig. 3c–e). Activation of such kinases is a hallmark of cell cycle arrest and apoptosis. On this basis we examined the consequences of CKi and MitoCKi on apoptosis initiation and found that both molecules robustly induced apoptosis (Figure 4f,g & Extended Data Fig. 4a & 5a,b). Importantly, this phenotype matched closely to those previously observed by genetic depletion of CKMT1 in UCSD-AML1 cells, providing further evidence for on-target toxicity on CKs by CKi and MitoCKi[2]. Moreover, as predicted we observed that both CKi and MitoCKi increased the

proportion of cells in G0/G1, as well as G2/M, suggestive of arrest of growth and mitosis (Figure 4h,i Extended Data Fig. 4b & 5c,d). In addition, CKi and MitoCKi treatment of non-CK reliant A549 cells resulted in no detectable effects on apoptosis or analogous effects on cell cycle arrest (Figure 4f–i & Extended Data Fig. 4 & 5). To confirm whether the above-described effects were attributable to energetic consequences of CKi, as opposed to direct effects on the kinome, we evaluated the kinome-wide selectivity of CKi using the commercially available DiscoverX KINOMEscan profiling platform consisting of 468 kinases (Extended Data Fig. 6a and Supplementary Table 8). We only found MKK7 to be a modest off-target (9.7 % DMSO control). Together our findings suggest that CKi and MitoCKi effectively deplete the creatine phosphagen system to arrest cell growth and initiate apoptosis in EVI1-positive AML.

CKs in control pro-inflammatory cytokine production.

Our data so far have demonstrated that CKi and MitoCKi are effective inhibitors of creatine phosphagen energetics in cells. In light of this, we predicted that these molecules would be useful to probe the importance of CKs generally in cell biological processes. Historically, the relevance of creatine energetics in cellular processes has been stifled by the lack of specific tools for efficient inhibition of the four CK isoforms, and laborious genetics required to genetically manipulate multiple CKs. To exemplify whether CKi and MitoCKi could be used to rapidly probe the relevance of creatine energetics, we examined macrophages. These cells exhibit distinct energetic requirements, in particular when producing cytokines in response to a pro-inflammatory stimulus. However, the importance of creatine phosphagen energetics in the macrophage inflammatory response has not been examined.

We applied CKi acutely to mouse bone marrow derived macrophages (BMDM) and human THP1 monocytes, which was sufficient to rapidly deplete cellular phosphocreatine (Figure 5a,b). Next, we stimulated pro-inflammatory cytokine production by application of LPS, which drove significant elevation of IL1β, IL6, and TNFα (Figure 5 c,d). Remarkably, inhibition of creatine kinases by CKi resulted in a selective remodeling of the pro-inflammatory cytokine response. In both BMDMs and THP1s, elevation of *Il1b* transcript was significantly inhibited upon depletion of creatine phosphagen system (Figure 5c,d). A similar effect was observed for *Il6*, albeit less pronounced (Figure 5c,d). In contrast, inhibition of CKs potentiated expression of *Tnf* upon stimulation by LPS (Figure 5c,d). To examine this phenomenon in greater detail, we explored the effects of CKi on acute signaling pathways and proteome response to LPS stimulation in THP1 cells. Notably, CKi did not affect canonical TLR signaling as assessed by monitoring IκBα abundance and phosphorylation status upon LPS stimulation (Extended Data Fig. 6b). To examine the pathways underlying CKi effects cytokine production, we profiled proteome and phospho-proteome changes induced by CKi following stimulation by LPS (Figure 5e,f & Supplementary Table 9,10). CKi affected the abundance and phosphorylation status of a small number of targets, including several established factors that regulate cytokine production. Among the most highly induced proteins by CKi was HMOX1, a protein well known to inhibit pro-inflammatory cytokine production[27]. Conversely, abundance of carbonic anhydrase 2 (CA2) was significantly depleted upon CKi. Interestingly,

inhibition of CA2 has been shown to repress pro-inflammatory cytokine production in macrophages[28]. CKi modulated phosphorylation status of a small number of known cytokine regulators, including SIK3 and CAMK1[29,30] (Figure 5f). Together, these data demonstrate a previously unappreciated role for the creatine phosphagen system in acute control over pro-inflammatory cytokine production, indicating that this pathway could be targeted to therapeutically manipulate inflammatory processes. Moreover, proteomic analyses identify established protein regulators of cytokine production that appear responsive to acute depletion of creatine energetics. More generally, our findings illustrate how CKi can be used to rapidly probe the relevance of CK activity in regulating cell biological processes.

Discussion.

CKs play a central role in coordinating energetic supply and demand in cells. By coordinating rapid and reversible generation of ATP from creatine phosphate, this enzyme family appears to be broadly relevant for meeting local energetic demand under conditions of unusually high ATP utilization. In this light, the creatine phosphagen system has emerged as a major metabolic liability of numerous cancers that rely on creatine phosphate derived ATP to support survival and growth. This work describes the development of potent and selective inhibitors of CK isozymes through selective targeting of a conserved active-site cysteine. The exemplars, CKi and MitoCKi, inhibit the CK phosphotransfer reaction and effectively deplete creatine phosphate in cells. Using the recently developed CPT reagent, we demonstrate that CKi engagement with CK active site cysteines is highly selective proteome wide in living cells. Rapid and potent inhibition of creatine kinases allows for examination of the role of creatine phosphagen energetics in biological systems using CKi and MitoCKi. In this work, we exemplify how this series of molecules are potently cytotoxic to CK-dependent AML cells, demonstrating a therapeutic rationale for targeting CKs in CK-reliant cancers. Moreover, having demonstrated the structural basis for CKi-mediated inhibition of CKs, a clear path exists for development of inhibitors for *in vivo* studies. Our current data suggest that CKi and derivatives are relatively unstable following intravenous injection, and so future studies will focus on improving pharmacokinetic and pharmacodynamic properties of these molecules for application to animal models of physiology and disease. Finally, we demonstrate how CKi and MitoCKi can be used to determine the relevance of creatine kinase energetics in regulating biological processes. Historically, these questions have been difficult to address because of the redundancy of multiple CK isoforms rendering genetic analysis laborious. Using CKi and MitoCKi we examine the role of creatine kinases in macrophage and monocyte energetics and uncover a previously unappreciated and substantial role for the creatine phosphagen system in supporting pro-inflammatory cytokine production. These findings suggest that this energetic couple could be effectively targeted to regulate macrophage-driven inflammation. More generally, CKi and MitoCKi allow for examination of creatine phosphagen utilization in cells and its relevance to biological processes.

Methods

Data Availability statement.

The datasets generated during and/or analyzed during the current study are available as Excel spreadsheets in Supplementary Tables 1–10. Source data are provided with this paper. All additional data is available upon request to the corresponding authors.

Gel based screening of CKB.

Ramos cell line was obtained from ATCC and grown at 37 °C with 5% CO_2 in RPMI-1640 media (Corning) supplemented with 10% fetal bovine serum (FBS, Omega Scientific), penicillin (100 U/mL), streptomycin (100 mg/mL), and L-glutamine (2 mM). The cells were grown to 1×10^6 cells/mL, then collected (3 min × 1400 *g*), washed with cold PBS (2 × 10mL), flash frozen in liquid nitrogen, and kept at −80 °C until further analysis. Cell pellets were lysed by sonication in PBS, fractionated into soluble and membrane proteomes by ultracentrifugation (45 min × 100,000 *g*), and the soluble fraction was used for the experiment. The resulting proteome was normalized to 1 mg/mL and doped with WT CKB or CKB_C283A (Final concentrations: 1 μM, 500 nM, 250 nM, 100 nM, 10 nM). iodoacedamide-rhodamine (2 μM) was added and the reaction was incubated for 1 h at rt. The labeling was visualized using SDS-PAGE gel following quenching with the 4x SDS-loading buffer and heating at 95 °C for 5 min. The compound screen was performed by pre-treatment of cell lysates (doped with CKB, 250 nM) with covalent electrophiles (20 μM) for 1 h before visualization with the iodoacetamide probe.

CPT chemoproteomics:

CPT synthesis and cysteine peptide enrichment was performed as described previously[17], with the exception that cell pellets were lysed and labeled using 50 mM HEPES, 2% SDS, 5 mM TCEP, and 10 mM CPT at pH 8.5. Protein digestion, TMT labelling and IMAC enrichment were done as described previously[17].

Proteomics & Phosphoproteomics:

Sample lysis, peptide preparation, phosphopeptide enrichment and quantitative phosphoproetomics was performed as described previously[31].

Kinase pathway analysis:

We used a recently developed database that systematically determined kinase substrate specificity for 303 kinases across the kinome (Manuscript in preparation). Briefly, each of 303 kinases was screened for phosphorylation activity against a peptide library of peptide substrates. We utilized synthetic peptide libraries, containing 198 peptide mixtures, that explored amino acid preference up to 5 residues N-terminal and C-terminal to the phosphorylated Ser/Thr to determine the optimal substrate sequence specificity for recombinant Ser/Thr kinases. In total, 303 kinases were profiled. Their motifs were quantified into position specific scoring matrices (PSSMs) and then applied computationally to score phosphorylation sites based on their surrounding amino acid sequences. These PSSMs were ranked against each site to identify the most favorable kinases. Reagents used

for the peptide library experiments include: Kinase substrate library (Anaspec). Streptavidin conjugated membranes (Promega). To determine the substrate motifs, we performed *in vitro* phosphorylation assays with recombinant kinases on the oriented peptide array library in the presence of ATP[γ–^{32}P] (Perkin-Elmer). The peptides were spotted onto streptavidin-coated filter sheets (Promega SAM^2 biotin capture membrane) and visualized by phosphorimaging on Typhoon FLA 7000. Detailed information on the protocol is provided elsewhere[32,33].

Matrix processing and substrate scoring. The matrices were normalized by the sum of the 17 randomized amino acids (all amino acids except for serine, threonine and cysteine), to yield a position specific scoring matrix. The serine, threonine and cysteine columns were scaled by their median to be 1/17. For scoring substrates, the values of the corresponding amino acids in the corresponding positions were multiplied and scaled by the probability of a random peptide:

$$\text{Score}_{\text{Kin X}} = \frac{\prod_{\text{Pos}} P_{\text{Kin X}}(\text{AA}, \text{Position})}{(1/\#\text{Random AA})^{\text{length(positions)}}}$$

For the percentile score of a substrate by a given kinase, we first computed the *a-priori* score distribution of that kinase by scoring all the reported S/T phosphorylation sites on PhosphoSitePlus by the method discussed above. The percentile score of a kinase-substrate pair is defined as the percentile ranking of the substrate within the score distribution of the given. This value is being used when analyzing all the detected phosphorylation sites (viral and host) for kinase enrichment

LC-MS/MS parameters and data processing:

LC-MS/MS and data processing was performed as previously described[17,31].

Metabolite profiling:

After treating cells with CKi or MitoCKi, cells were collected and washed with PBS. 250 µL of 80% MeOH containing 0.05 ng/µL thymine-D4, 0.05 ng/µL ^{15}N4-inosine, and 0.10 ng/µL glycocholate-D4 was added to the cell pellet and vortexed. Cell debris was removed by centrifugation for 10 mins, 15,000 × g, 4 °C. The supernatant was transferred into a fresh tube and centrifuged again. The supernatant was collected and subjected to LC-MS analysis as described previously[31]. Briefly, metabolite extracts were loaded onto a Luna-HILIC column (Phenomenex) with 10% mobile phase A (20 mM ammonium acetate and 20 mM ammonium hydroxide in water) and 90% mobile phase B (10 mM ammonium hydroxide in 75:25 v/v acetonitrile/methanol). Analysis was carried out using a QExactive HF-X mass spectrometer (Thermo Fisher Scientific). Negative and positive ion modes were used with full scan analysis over m/z 70–750 m/z at 60,000 resolution, 1e6 AGC, and 100 ms maximum ion accumulation time. Targeted processing of a subset of known metabolites was conducted using TraceFinder software version 4.1 (Thermo Fisher Scientific). Compound identities were confirmed using reference standards. In all cases metabolite abundance was normalized using internal standards and relative changes were assessed by comparison with metabolite extracted from the same sample type.

Protein expression and purification:

The N-terminal His tag construct of human CKB (residues 1–381) was overexpressed in E. coli BL21 (DE3) and purified using affinity chromatography and size-exclusion chromatography. Briefly, cells were grown at 37°C in TB medium in the presence of 50 μg/ml of kanamycin to an OD of 0.8, cooled to 17°C, induced with 500 μM isopropyl-1-thio-D-galactopyranoside (IPTG), incubated overnight at 17°C, collected by centrifugation, and stored at −80°C. Cell pellets were lysed in buffer A (25 mM HEPES, pH 7.5, 500 mM NaCl, 7 mM mercapto-ethanol, and 20 mM Imidazole) using Microfluidizer (Microfluidics), and the resulting lysate was centrifuged at 30,000g for 40 min. Ni-NTA beads (Qiagen) were mixed with cleared lysate for 30 min and washed with buffer A. Beads were transferred to an FPLC-compatible column, and the bound protein was washed further with buffer A for 10 column volumes and eluted with buffer B (25 mM HEPES, pH 7.5, 500 mM NaCl, 7 mM mercapto-ethanol, and 400 mM Imidazole). The eluted sample was concentrated and purified further using a Superdex 200 16/600 column (Cytiva) in buffer C containing 20 mM HEPES, pH 7.5, 200 mM NaCl, 5% glycerol, 1mM DTT and 0.5 mM TCEP. CKB containing fractions were concentrated to ~50 mg/mL and stored in −80°C.

Crystallization:

A sample of 1 mM protein and 1 mM CKi was crystallized in 1.7M Ammonium citrate, pH 7.4 NH_4Citrate pH 6 by sitting-drop vapor diffusion at 20dc. Crystals were transferred briefly into a crystallization buffer containing 25% glycerol or Mix4 (18% Glycerol, 18% Ethylene Glycol, 20% Sucrose, 4% Glucose) prior to flash-freezing in liquid nitrogen.

Data collection and structure determination:

Diffraction data were collected at beamline 24ID-E of the NE-CAT at the Advanced Photon Source (Argonne National Laboratory). Data sets were integrated and scaled using XDS[34]. Structures were solved by molecular replacement using the program Phaser[35] and the search model PDB entry 3DRE. Iterative manual model building and refinement using Phenix[36] and Coot[37] led to a model with excellent statistics.

Recombinant CKB cysteine site engagement:

DMSO or 1.25 mM CKi was added to 25 μM recombinant CKB (in 50 mM TRIS pH 9) and incubated for 2 h at 37 °C. Afterwards, a mixture of 5 μL of 20% SDS, 5 μL of 500 mM iodoacetamide, 0.5 μL of TCEP, 2.5 μL of 1 M TRIS pH 9, and 12 μL of water was added and incubated for 1 h in the dark. The mixture was then subjected to methanal chloroform precipitation and the resulting pellet was washed with methanol. 50 uL of EPPS, pH 8, 0.5 μg trypsin, and 0.5 ug Lys-C was added to the protein pellet and the solution was incubated overnight at 37 °C. Digested peptides were subjected to tandem mass tag (TMT)-labeling following manufacturers' instructions. Briefly, to 14 μL of sample, 2 μL of respective TMT and 4 μL of acetonitrile was added. After incubating for 1 h, the reaction was quenched using 5% hydroxylamine for 15 min and acidified using 20% formic acid. All channels were then pooled, diluted to 5% acetonitrile using 1% formic acid, desalted using Sep-Pak C18 cartridges, and lyophilized overnight. The sample was resuspended with 5% formic

acid in 5% acetonitrile, and analyzed by LC-MS. Data analysis was performed as described previously[17].

Intact protein mass spectrometry:

1 μL of CKi (100x stock) was added to 50 μL of 800 nM human recombinant CKB and incubated for 2 h (or indicted time) at 37 °C. Then, the sample was subjected to LC-MS analysis using a PLRP-S 1000A, 2.1 × 50 mm, 5 um (Agilent) column on a Q-Exactive HF-X. The buffers used for separation was 2% formic Acid in water (Buffer A) and 2% Formic Acid in acetonitrile (Buffer B) which was run at 0.3 mL/min at 60 °C. The gradient was 15% B for 0.5 mins, followed up by ramping up to 95% over 4.5 mins. Positive ion modes were collected with full scan analysis over m/z 900–2600 m/z at 7,500 resolution, 1e5 AGC, 25 ms maximum ion accumulation time and 60 eV in-source CID. Data processing was conducted using Thermo Biopharma Finder software version 4.1 (Thermo Fisher Scientific).

Biotin enrichment and western blotting:

UCSD-AML1 cells were treated with alkyne-CKi, or CKi, as indicated and collected by centrifuging for 2 min at 2,000 g. The pellets were washed with PBS twice and then subjected to lysis and biotin enrichment as described previously[38]. For CKi pretreated samples, cells were lysed using 1% Triton X-100, 50 mM TRIS, 150 mM NaCl, 10 μM Alkyne-CKi at pH 7.4 and incubated for 1 hour at 37 °C before subjecting samples to biotin enrichment as described above.

Creatine kinase activity:

Recombinant CKB was diluted to 250 nM using 50 mM TRIS, 100 μM TCEP, pH 9, and 20 μL was added to each well of a 384 well plate. Small molecules or DMSO were added at indicated final concentrations and incubated for 2 h (or indicted time) at 37 °C. Next, samples were diluted into assay buffer with the following final concentrations: 100 nM CKB, 40 μM TCEP, 3 mM ATP, 1.2 mM PEP, 12 mM $MgCl_2$, 210 μM NADH, 60 mM KCl, 50 mM TRIS, 9 units/mL Pyruvate Kinase, 4.2 units/mL L-Lactate Dehydrogenase, and 6 mM creatine at pH 9. The absorbance was measured at a wavelength of 340 nm over 30 mins.

Cellular viability:

Cellular viability was performed as described previously[2]. Briefly, UCSD-AML1 or A549 cells were diluted to 20,000 cells ml^{-1}. After 24 h, molecules or DMSO were added at indicated concentrations. After 3 days, CellTiter-Glo Luminescent Cell Viability Assay was performed according to the manufacturer's instructions.

Assessment of apoptosis:

Apoptosis assessments were performed as described previously[2]. Briefly, after treating UCSD-AML1 or A549 for 16 h with 10 CKi or MitoCKi, cells were harvested and subjected to APC Annexin V Apoptosis Detection Kit with 7-AAD (BioLegend Cat#640930) in according to the manufacturer's instructions.

Assessment of cell cycle:

Cell cycle assessments were performed as described previously[2]. Briefly, after treating UCSD-AML1 or A549 for 16 h with 10 CKi or MitoCKi, cells were harvested and subjected to Click-iT Plus EdU Alexa Fluor 647 Flow Cytometry Assay Kit (ThermoFisher Scientific Cat# C10634) in accordance with manufacture's protocol. The kit was supplemented with FxCycle Violet Stain (ThermoFisher Scientific Cat# F10347) during the optional stain cells for DNA content step.

Kinome Profiling:

Protocols for the KINOMEscan are available from DiscoverX. Treespot images were generated, using TREEspot Software Tool, and reprinted with permission from KINOMEscan, a division of DiscoverX Corporation, DISCOVERX CORPORATION 2010. CKi was tested at a concentration of 10 μM.

Generation of BMDMs:

Mice were euthanized by CO_2 and bone marrow cells were extracted from the leg bones and differentiated in DMEM (containing 10% fetal calf serum, 1% penicillin/streptomycin and 20% L929 supernatant) as described previously[39]. Image generated using TREEspot™ Software Tool and reprinted with permission from KINOMEscan®, a division of DiscoveRx Corporation, © DISCOVERX CORPORATION 2010.

Treatment and analysis of BMDMs and THP1 cells:

5×10^6 BMDMs or THP1/ml were used for experiments. LPS concentration used was 100 ng ml^{-1}. CKi and MitoCKi were applied for 2 hr prior to LPS or vehicle for 6 hr at stated concentrations. Total RNA was extracted using TRIzol (Invitrogen), and purified with Pure RNA Mini Kit (Invitrogen). Then 1.5 μg of RNA was subjected to reverse transcription-polymerase chain reaction using a high-capacity cDNA reverse transcription kit. Using SYBR green probe, qPCR was performed on a 7900 HT Fast Real-Time PCR System (Applied Biosystems) using GoTaq qPCR Master Mix (Promega). The primers used for quantification were: Mice IL1B FWD 5'-TGG CAA CTG TTC CTG-3" REV 5'-GGA AGC AGC CCT TCA TCT TT-3'. Mice IL6 FWD 5'-ACA AAG CCA GAG TCC TTC AGA GAG-3" REV 5'-TTG GAT GGT CTT GGT CCT TAG CCA-3'. Mice TNF-a FWD 5'-GCC TCT TCT CAT TCC TGC TT-3" REV 5'-TGG GAA CTT CTC ATC CCT TTG-3'. Mice RPS18 FWD 5'-GGA TGT GAA GGA TGG GAA GT-3" REV 5'-CCC TCT ATG GGC TCG AAT TT-3'. Human IL1B FWD 5'-AGC TGA TGG CCC TAA ACA CA-3" REV 5'-TGT CCA TGG CCA CAA CAA CTG A-3'. Human IL6 FWD 5'-TCT GGA TTC AAT GAG GAG ACT TG-3" REV 5'-CTC AAA TCT GTT CTG GAG GTA CT-3'. Human TNF-a FWD 5'-CCA GGG ACC TCT CTCT AAT CA-3" REV 5'-TCA GCT TGA GGG TTT GCT AC-3'.Human Beta-Actin FWD 5'-CAC AGA GCC TCG CCT TT-3" REV 5'-GAG CGC GGC GAT ATC AT-3'

Overexpression of CKB in HEK293.

Control or 3xFlag-CKB lentiviral expression vectors (pLX-GFP) were obtained from Genetic Perturbation Platform at the Broad Institute or VectorBuilder Inc. Virus was

produced using HEK293T transfected with lentiviral expression vectors, together with envelope VSVG and the gag-pol psPAX2 constructs. For transduction, viral supernatant was added onto HEK293T cells seeded in a 6-well plate, and polybrene was added at 8 μg/mL. Then cells were centrifuged in viral supernatant at 1000 g for 1hr at 33 °C and allowed to grow for 3 days.

Analysis by in-gel fluorescence:

After treating UCSD-AML1 with CKi-Alk or Iodo-ALk for 16 h, cells were then processed as described previously[38] except the dye used was AZDye 800 Picolyl Azide and gels were scanned using Odyssey CLx (LI-COR).

CKi-Alk treated biotin enrichment and western blotting:

After treating cells with CKi-Alk for 16 h, cells were then processed as described previously[38] except azido-biotin was used and elution was performed by boiling sampling in 2x loading buffer for 5 min.

CKi-Alk treated lysate biotin enrichment and western blotting:

After treating cells with CKi for 16 h, cells were collected by centrifugation at 2,000 × g for 2 min, followed by washing with PBS. Cells were then suspended in 1% Triton X-100, 50 mM TRIS, 150 NaCl, pH 7.4 and sonicated. Cell debris was removed by centrifugation, protein concentration was determined using BCA, and normalized to 1 mg mL^{-1}. Then CKi-Alk was added and incubated for 1 h at 37 °C. Samples were then subjected to methanol chloroform precipitation and biotin enrichment as above.

Assessment of ATP/ADP Ratio:

After treating UCSD-AML1 for 16 h ± CKi, cells were harvested and subjected to ADP/ATP Ratio Assay kit (abcam Cat# ab65313) in according to the manufacturer's instructions.

Determination of K_{inact}/K_i:

CKi was added to 25 μL of 800 nM human recombinant CKB at indicated concentrations and incubated for indicted times at 37 °C. Following this, 75 μL of 5% formic acid, 5% acetonitrile, 50 mM 2-Mercaptoethanol was added and the sample was subjected to LC-MS as described above. After determining percent engagement using Thermo Biopharma Finder software version 4.1 (Thermo Fisher Scientific), K_{inact}/K_i was determine as described previously[40].

Chemical synthesis:

See Supplementary Information.

Extended Data

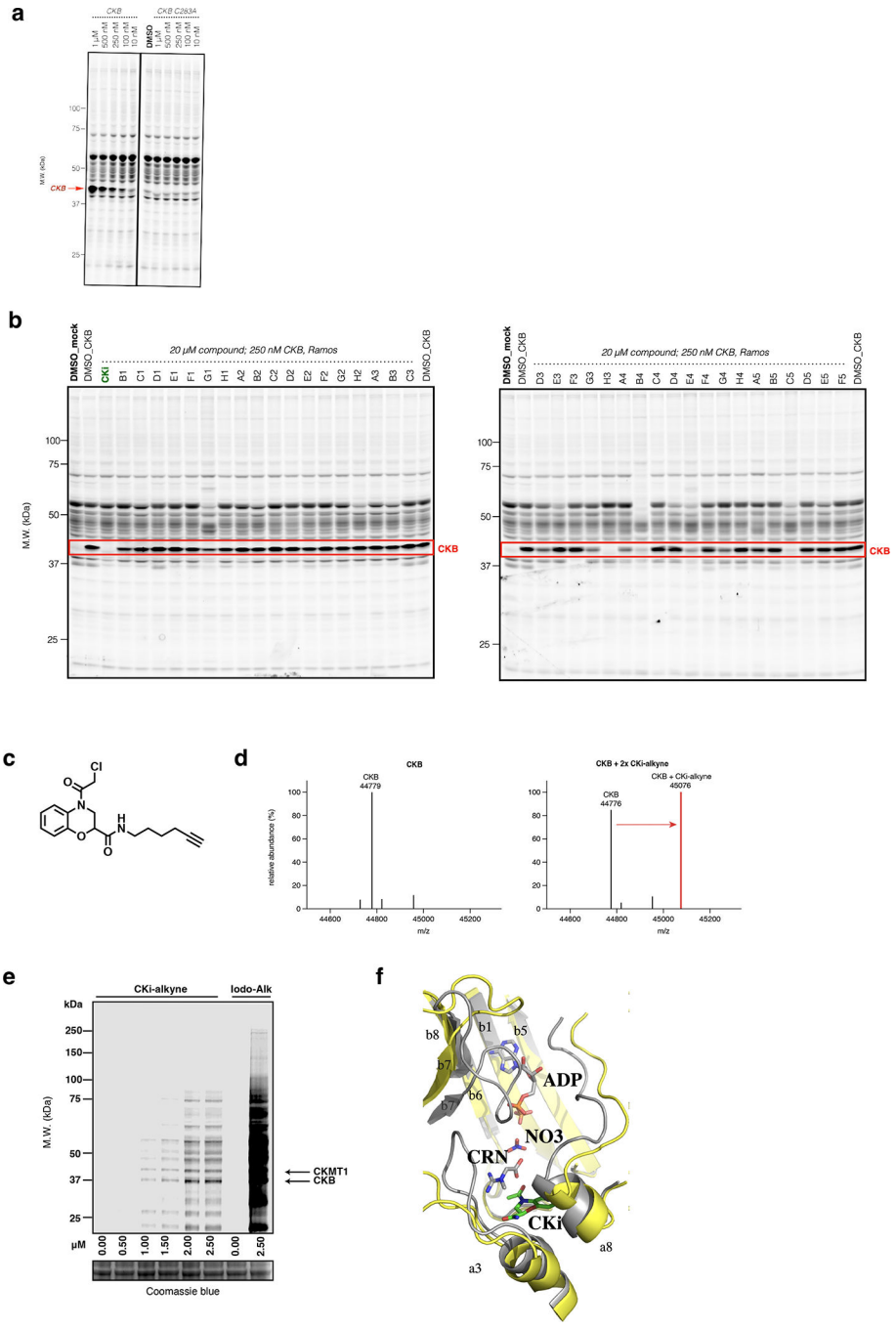

Extended Data Fig. 1. Characterizing CKi interaction with CKB

(a) Establishing gel-based screening of recombinant CKB in Ramos cell lysates for engagement of cysteine 283 by competition labeling with iodoacetamide-rhodamine. Single experiment shown.

(b) Fragment competition labeling of recombinant CKB in Ramos cell lysates identifies small molecules that compete with iodoacetamide-rhodamine labeling. CKi is highlighted in green. Single experiment shown

(c) Structure of CKi-alkyne.

(d) Left: Intact protein MS of 800 nM human recombinant CKB incubated for 2 h with DMSO at 37 °C. Right: Intact protein MS of 800 nM human recombinant CKB incubated for 2 h with 1.6 μM CKi-alkyne at 37 °C.

(e) UCSD-AML1 cells incubated with alkyne-CKi followed by conjugation to flouorophore for gel based detection. Fluorophore-conjugated iodoacetamide included as a promiscuous labeling control.

(f) Crystal structure active site of human CKB bound to CKi highlighting Cys283, ADP, creatine, location of ligands based on PDB: 3B6R

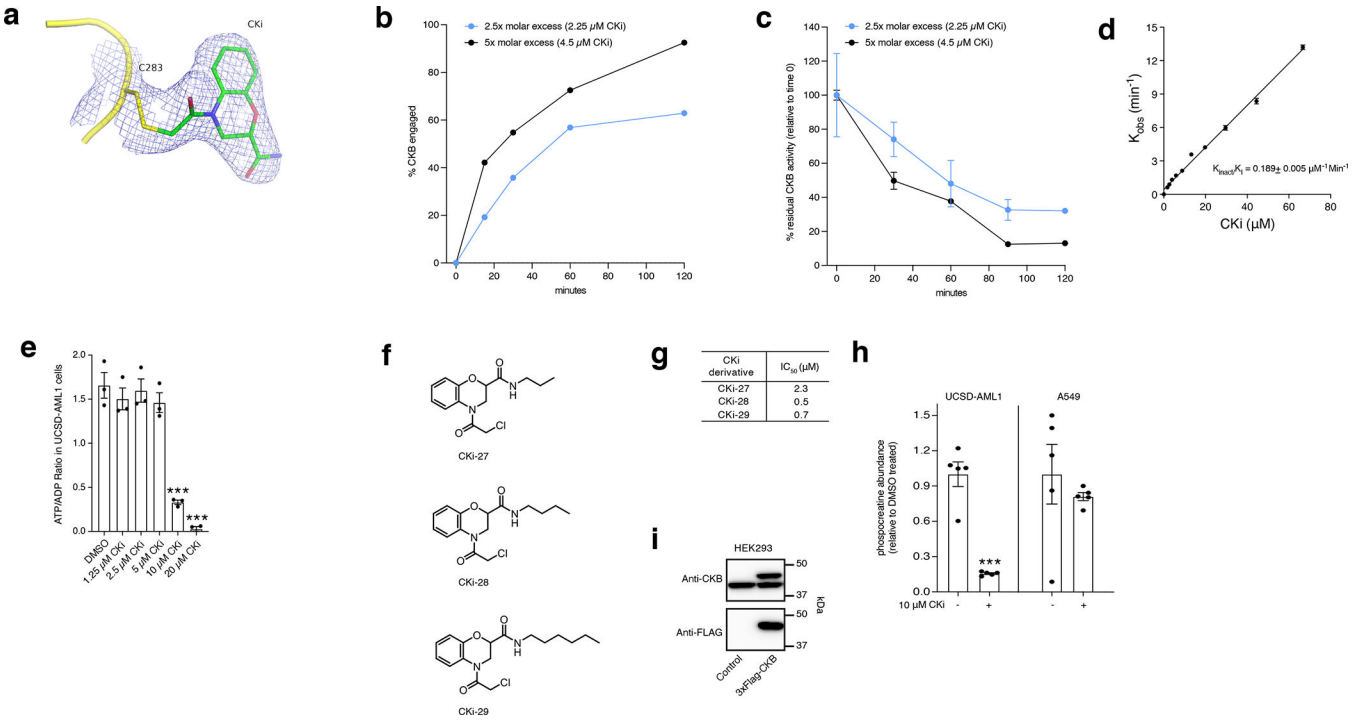

Extended Data Fig. 2. Effects of CKi on recombinant CKB

(a) Electron density of CKi in the active site of CKB. A 2FO-FC map of CKi and its attached residue (Cys283) at sigma 1.0.

(b) % CKi engagement with human recombinant CKB assessed by monitoring intact mass of CKB over 2 h at 37 °C.

(c) Recombinant CKB phosphotransfer activity ± incubation with CKi for indicated times. n=3 independent experiments.

(d) K_{inact}/K_i determined using % CKi engagement with human recombinant CKB assessed by monitoring intact mass of CKB over 2 h at 37 °C at different concentrations of CKi. n=3.

(e) ATP/ADP ratio determined in UCSD-AML1 after treating with 0, 1.25, 2.5 5, 10, and 20 μM CKi for 16 h using ADP/ATP ratio assay kit. n = 3 biological cell replicates.

(f) Structure of select CKi analogs with increasing hydrocarbon lengths.

(g) Recombinant CKB phosphotransfer activity ± 2 h preincubation with CKi analogs with increasing hydrocarbon length.

(h) Creatine and phosphocreatine abundance in UCSD-AML1 and A549 cells treated with 10 μM CKi. n=5.

(i) HEK293 cells over-expressing (OE) Flag-CKB exhibit significant increase in total cellular CKB content. Representative blot from 2 independent experiments shown.

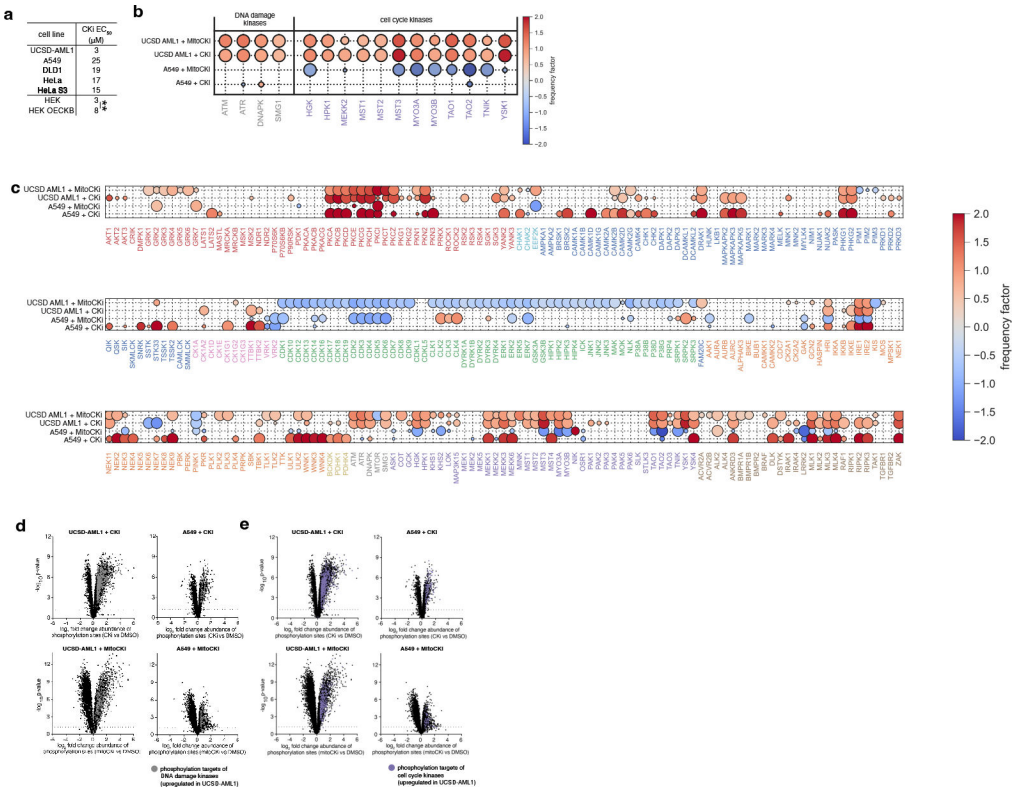

Extended Data Fig. 3. Phosphoproteome remodeling induced by CKi and MitoCKi

(a) The effect of CKi on cell viability in a range of cancer cell lines. HEK; HEK293 cells, HEKOECKB are cells generated in Extended Data Fig. 2i. n=8.

(b) Cell type specific phosphoproteomic signature of UCSD-AML1 and A549 cells treated for 16 h with 10 μM CKi or 5 μM MitoCKi. n=5.

(c) Full phosphoproteomic analysis of UCSD-AML1 or A549 cells treated with 10 μM CKi or 5 μM MitoCKi for 16 h. (n=5). Upregulated and downregulated sites were then subjected to kinase enrichment analysis as describe in Methods.

(d) Volcano plots showing phosphoproteomic analysis of UCSD-AML1 or A549 cells treated with 10 μM CKi or 5 μM MitoCKi for 16 h. n=5.

(e) Volcano plots showing phosphoproteomic analysis of UCSD-AML1 or A549 cells treated with 10 μM CKi or 5 μM MitoCKi for 16 h. n=5.

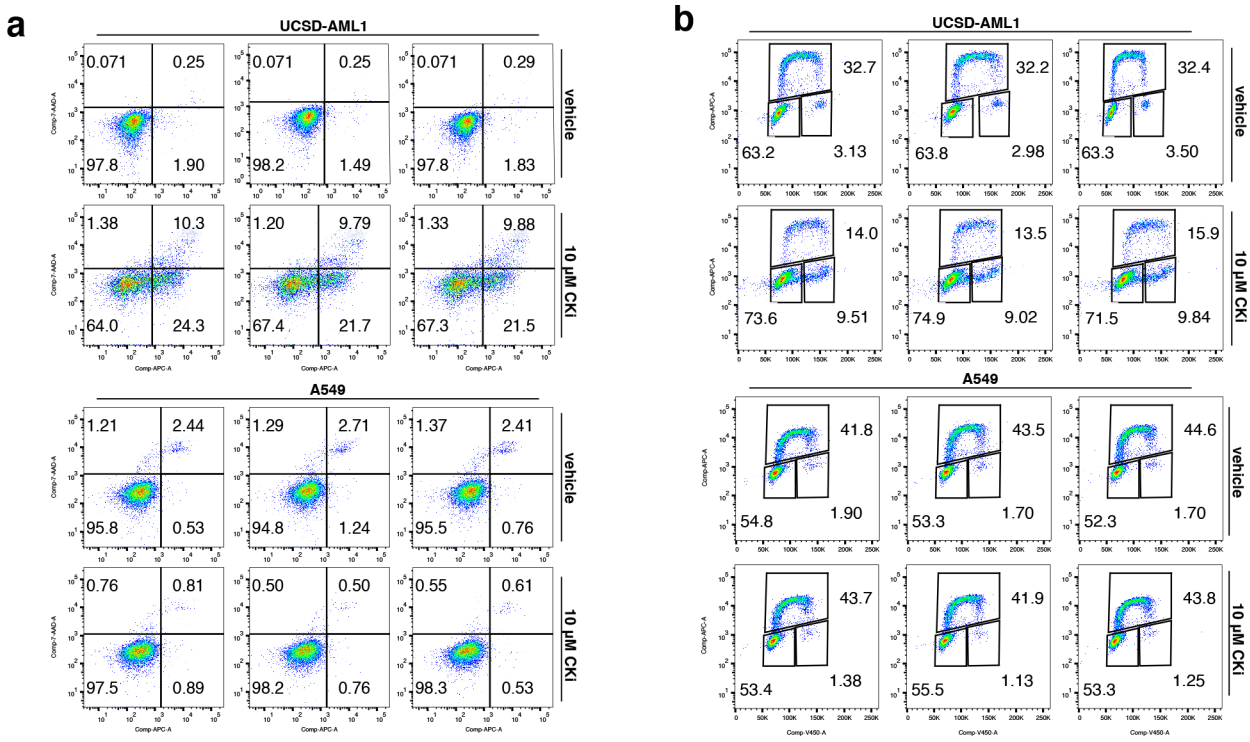

Extended Data Fig. 4. CKi flow cytometry analysis

(a) Flow cytometry analysis using Annexin V and 7-AAD staining of UCSD-AML1 or A549 cells treated with DMSO or 10 μM CKi for 16 h. n=3.

(b) Flow cytometry analysis using Click-iT Plus EdU Alexa Fluor 647 and FxCycle Violet staining of UCSD-AML1 or A549 cells treated with DMSO or 10 μM CKi for 16 h. n=3.

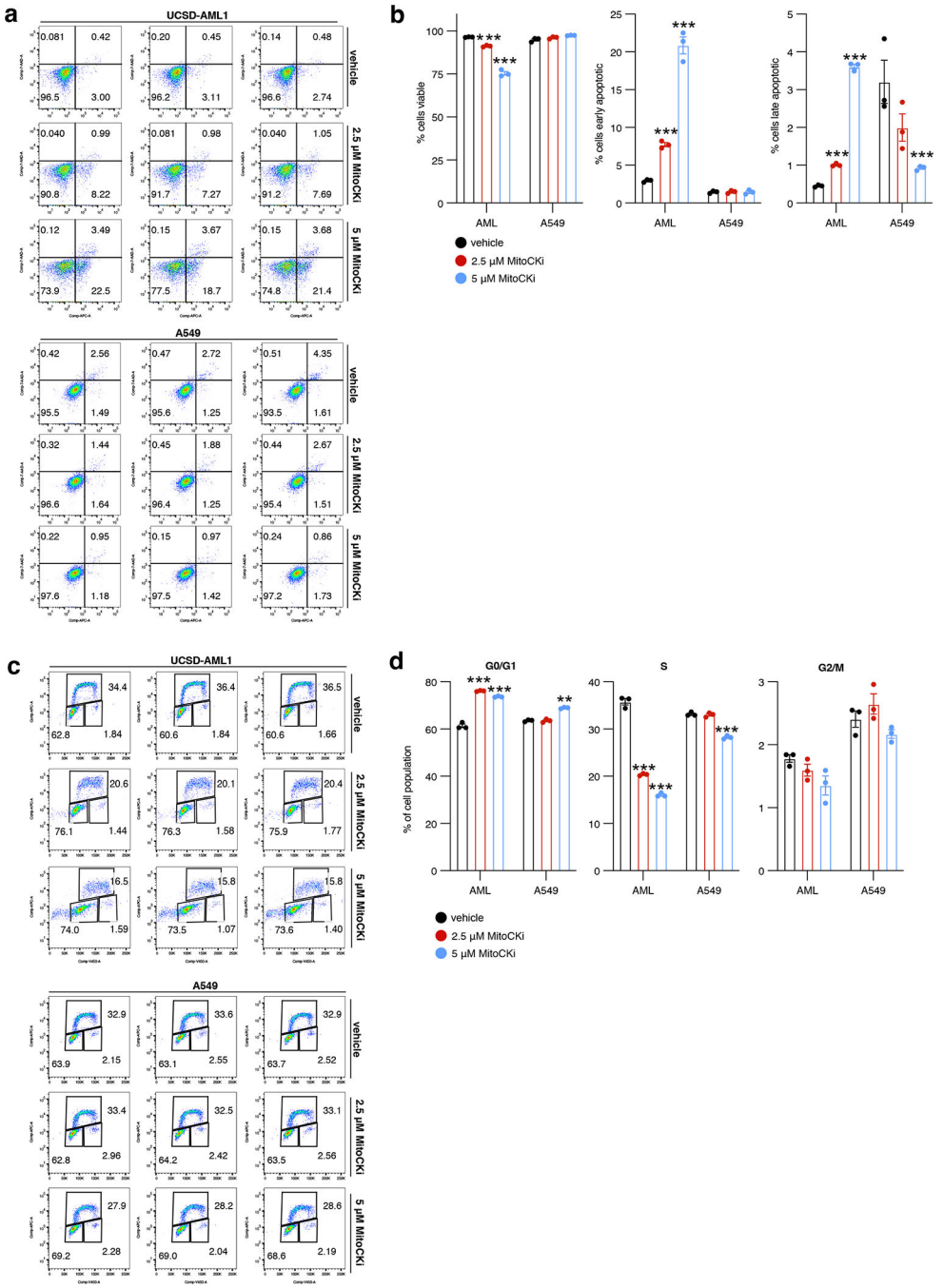

Extended Data Fig. 5. CKi and MitoCKi flow cytometry analyses

(a) Flow cytometry analysis using Annexin V and 7-AAD staining of UCSD-AML1 or A549 cells treated with DMSO, 2.5 or 5 μM MitoCKi for 16 h.

(b) Quantification of fraction of cells that are apoptotic after 16 h of treatment with DMSO, 2.5 or 5 μM MitoCKi. n=3.

(c) Flow cytometry analysis using Click-iT Plus EdU Alexa Fluor 647 and FxCycle Violet staining of UCSD-AML1 or A549 cells treated with DMSO, 2.5 or 5 μM MitoCKi for 16 h.

(d) Quantification of fraction of cells that are in S, G0/G1 and G2/M phase of the cell cycle after 16 h of treatment with DMSO, 2.5 or 5 μM MitoCKi. n=3.

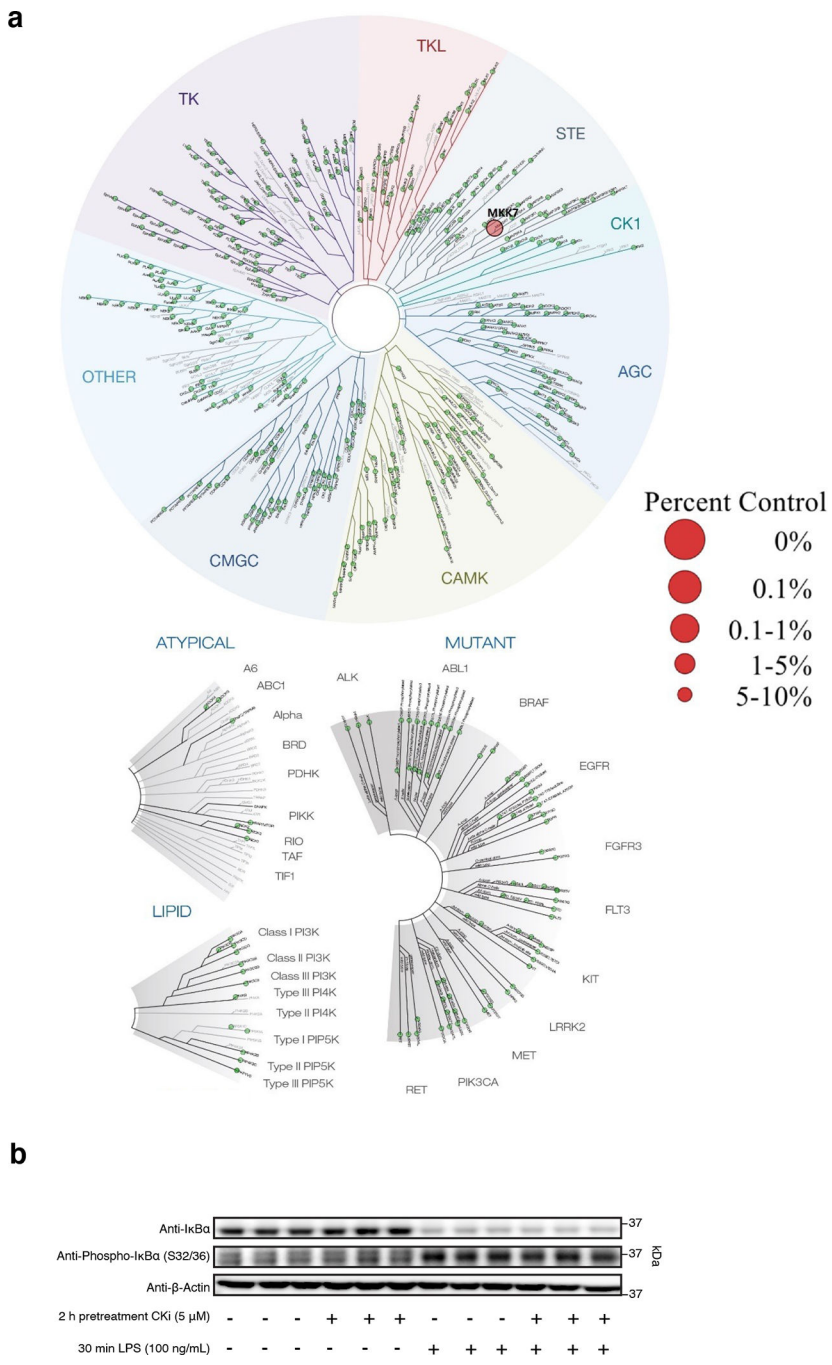

Extended Data Fig. 6. Kinome analysis and TLR pathway analysis of CKi

(a) Kinome-wide selectivity profile for compound CKi at 10 μM. CKi was tested at 10 μM on a panel of 468 kinases (Creatine Kinases are not in the panel). The results are displayed as red circles with their sizes correlating with the inhibitor's binding affinity (percent DMSO control). Complete dataset is included in Table S7.

(b) Immunoblot of IκBα and phosphorylated IκBα in THP1 cells ± CKi and ± LPS. Representative blot from 3 independent experiments shown.

Supplementary Material

Refer to Web version on PubMed Central for supplementary material.

Acknowledgements:

This work was supported by the Claudia Adams Barr Program (E.T.C), the Lavine Family Fund (E.T.C), the Pew Charitable Trust (E.T.C), NIH CA259739-01 (E.T.C), AG071966-01 (E.T.C), NIH DK123095 (E.T.C), The Smith Family Foundation (E.T.C), T32CA236754 (N.D), the National Cancer Center (H.X. & N.D) NCI R35 CA210030 (K.St.) and P50 CA206963 (K.St.), K99AG073461 (H.X.), NCI R35 CA231991 (B.F.C.), the Linde Family Foundation (S.D.P), the Doris Duke Charitable Foundation (S.D.P), Deerfield 3DC (S.D.P), Taiho Pharmaceuticals (S.D.P), NCI K99 CA263161 (S.L). S.L. is a Fellow of the Leukemia & Lymphoma Society. This work was based upon research conducted at the Northeastern Collaborative Access Team beamlines, which were funded by the National Institute of General Medical Sciences from the National Institutes of Health (P30 GM124165). The Eiger 16M detector on the 24-ID-E beam line was funded by a NIH-ORIP HEI grant (S10OD021527). This research used resources of the Advanced Photon Source, a U.S. Department of Energy (DOE) Office of Science User Facility operated for the DOE Office of Science by Argonne National Laboratory under Contract No. DE-AC02-06CH11357.

References

1. Kazak L & Cohen P Creatine metabolism: energy homeostasis, immunity and cancer biology. Nat Rev Endocrinol 16, 421–436 (2020). [PubMed: 32493980]
2. Fenouille N, et al. The creatine kinase pathway is a metabolic vulnerability in EVI1-positive acute myeloid leukemia. Nature medicine 23, 301–313 (2017).
3. Loo JM, et al. Extracellular metabolic energetics can promote cancer progression. Cell 160, 393–406 (2015). [PubMed: 25601461]
4. Maguire OA, et al. Creatine-mediated crosstalk between adipocytes and cancer cells regulates obesity-driven breast cancer. Cell metabolism 33, 499–512.e496 (2021). [PubMed: 33596409]
5. Zhang L, et al. Creatine promotes cancer metastasis through activation of Smad2/3. Cell metabolism 33, 1111–1123.e1114 (2021). [PubMed: 33811821]
6. Papalazarou V, et al. The creatine–phosphagen system is mechanoresponsive in pancreatic adenocarcinoma and fuels invasion and metastasis. Nature Metabolism 2, 62–80 (2020).
7. Streijger F, et al. Mice lacking brain-type creatine kinase activity show defective thermoregulation. Physiol Behav 97, 76–86 (2009). [PubMed: 19419668]
8. Streijger F, et al. Structural and behavioural consequences of double deficiency for creatine kinases BCK and UbCKmit. Behav Brain Res 157, 219–234 (2005). [PubMed: 15639173]
9. Van der Zee C Hypothalamic plasticity of neuropeptide Y is lacking in brain-type creatine kinase double knockout mice with defective thermoregulation. Eur J Pharmacol 719, 137–144 (2013). [PubMed: 23891845]
10. Steeghs K, et al. Cytoarchitectural and metabolic adaptations in muscles with mitochondrial and cytosolic creatine kinase deficiencies. Mol Cell Biochem 184, 183–194 (1998). [PubMed: 9746321]
11. Kurth I, et al. Therapeutic targeting of SLC6A8 creatine transporter suppresses colon cancer progression and modulates human creatine levels. Sci Adv 7, eabi7511 (2021). [PubMed: 34613776]
12. Kazak L, et al. A Creatine-Driven Substrate Cycle Enhances Energy Expenditure and Thermogenesis in Beige Fat. Cell 163, 643–655 (2015). [PubMed: 26496606]
13. Bong SM, et al. Structural studies of human brain-type creatine kinase complexed with the ADP-Mg2+-NO3- -creatine transition-state analogue complex. FEBS Lett 582, 3959–3965 (2008). [PubMed: 18977227]

14. Shen YQ, Tang L, Zhou HM & Lin ZJ Structure of human muscle creatine kinase. Acta Crystallogr D Biol Crystallogr 57, 1196–1200 (2001). [PubMed: 11517911]
15. Fritz-Wolf K, Schnyder T, Wallimann T & Kabsch W Structure of mitochondrial creatine kinase. Nature 381, 341–345 (1996). [PubMed: 8692275]
16. Eder M, Fritz-Wolf K, Kabsch W, Wallimann T & Schlattner U Crystal structure of human ubiquitous mitochondrial creatine kinase. Proteins 39, 216–225 (2000). [PubMed: 10737943]
17. Xiao H, et al. A Quantitative Tissue-Specific Landscape of Protein Redox Regulation during Aging. Cell 180, 968–983 e924 (2020). [PubMed: 32109415]
18. Lu W, et al. Correction: Fragment-based covalent ligand discovery. RSC Chem Biol 2, 670–671 (2021). [PubMed: 34459829]
19. Backus KM, et al. Proteome-wide covalent ligand discovery in native biological systems. Nature 534, 570–574 (2016). [PubMed: 27309814]
20. Kuljanin M, et al. Reimagining high-throughput profiling of reactive cysteines for cell-based screening of large electrophile libraries. Nature biotechnology 39, 630–641 (2021).
21. Weerapana E, et al. Quantitative reactivity profiling predicts functional cysteines in proteomes. Nature 468, 790–795 (2010). [PubMed: 21085121]
22. Vinogradova EV, et al. An Activity-Guided Map of Electrophile-Cysteine Interactions in Primary Human T Cells. Cell 182, 1009–1026.e1029 (2020). [PubMed: 32730809]
23. Coles BF & Kadlubar FF Detoxification of electrophilic compounds by glutathione S-transferase catalysis: determinants of individual response to chemical carcinogens and chemotherapeutic drugs? Biofactors 17, 115–130 (2003). [PubMed: 12897434]
24. Li Q, et al. Insights into the Phosphoryl Transfer Mechanism of Human Ubiquitous Mitochondrial Creatine Kinase. Scientific reports 6, 38088 (2016). [PubMed: 27909311]
25. Smith RA, Hartley RC & Murphy MP Mitochondria-targeted small molecule therapeutics and probes. Antioxid Redox Signal 15, 3021–3038 (2011). [PubMed: 21395490]
26. Lillie JW, et al. Cyclocreatine (1-carboxymethyl-2-iminoimidazolidine) inhibits growth of a broad spectrum of cancer cells derived from solid tumors. Cancer Res 53, 3172–3178 (1993). [PubMed: 8319226]
27. Naito Y, Takagi T & Higashimura Y Heme oxygenase-1 and anti-inflammatory M2 macrophages. Archives of biochemistry and biophysics 564, 83–88 (2014). [PubMed: 25241054]
28. Hudalla H, et al. Carbonic Anhydrase Inhibition Ameliorates Inflammation and Experimental Pulmonary Hypertension. Am J Respir Cell Mol Biol 61, 512–524 (2019). [PubMed: 30951642]
29. Strowitzki MJ, et al. Carbon Dioxide Sensing by Immune Cells Occurs through Carbonic Anhydrase 2–Dependent Changes in Intracellular pH. J. Immunol, ji2100665 (2022).
30. Zhang X, et al. Calcium/calmodulin-dependent protein kinase (CaMK) Ialpha mediates the macrophage inflammatory response to sepsis. J Leukoc Biol 90, 249–261 (2011). [PubMed: 21372190]

Methods References:

31. Reddy A, et al. pH-Gated Succinate Secretion Regulates Muscle Remodeling in Response to Exercise. Cell (2020).
32. Hutti JE, et al. A rapid method for determining protein kinase phosphorylation specificity. Nature Methods 1, 27–29 (2004). [PubMed: 15782149]
33. Turk BE, Huang LL, Piro ET & Cantley LC Determination of protease cleavage site motifs using mixture-based oriented peptide libraries. Nature biotechnology 19, 661–667 (2001).
34. Kabsch W Integration, scaling, space-group assignment and post-refinement. Acta Crystallogr D Biol Crystallogr 66, 133–144 (2010). [PubMed: 20124693]
35. McCoy AJ, et al. Phaser crystallographic software. J Appl Crystallogr 40, 658–674 (2007). [PubMed: 19461840]
36. Adams PD, et al. PHENIX: a comprehensive Python-based system for macromolecular structure solution. Acta Crystallogr D Biol Crystallogr 66, 213–221 (2010). [PubMed: 20124702]

37. Emsley P & Cowtan K Coot: model-building tools for molecular graphics. Acta Crystallogr D Biol Crystallogr 60, 2126–2132 (2004). [PubMed: 15572765]

38. Darabedian N, Chen TC, Molina H, Pratt MR & Schönthal AH Bioorthogonal Profiling of a Cancer Cell Proteome Identifies a Large Set of 3-Bromopyruvate Targets beyond Glycolysis. ACS Chem Biol 13, 3054–3058 (2018). [PubMed: 30395437]

39. Mills EL, et al. Itaconate is an anti-inflammatory metabolite that activates Nrf2 via alkylation of KEAP1. Nature 556, 113–117 (2018). [PubMed: 29590092]

40. Pettinger J, Carter M, Jones K & Cheeseman MD Kinetic Optimization of Lysine-Targeting Covalent Inhibitors of HSP72. J Med Chem 62, 11383–11398 (2019). [PubMed: 31725295]

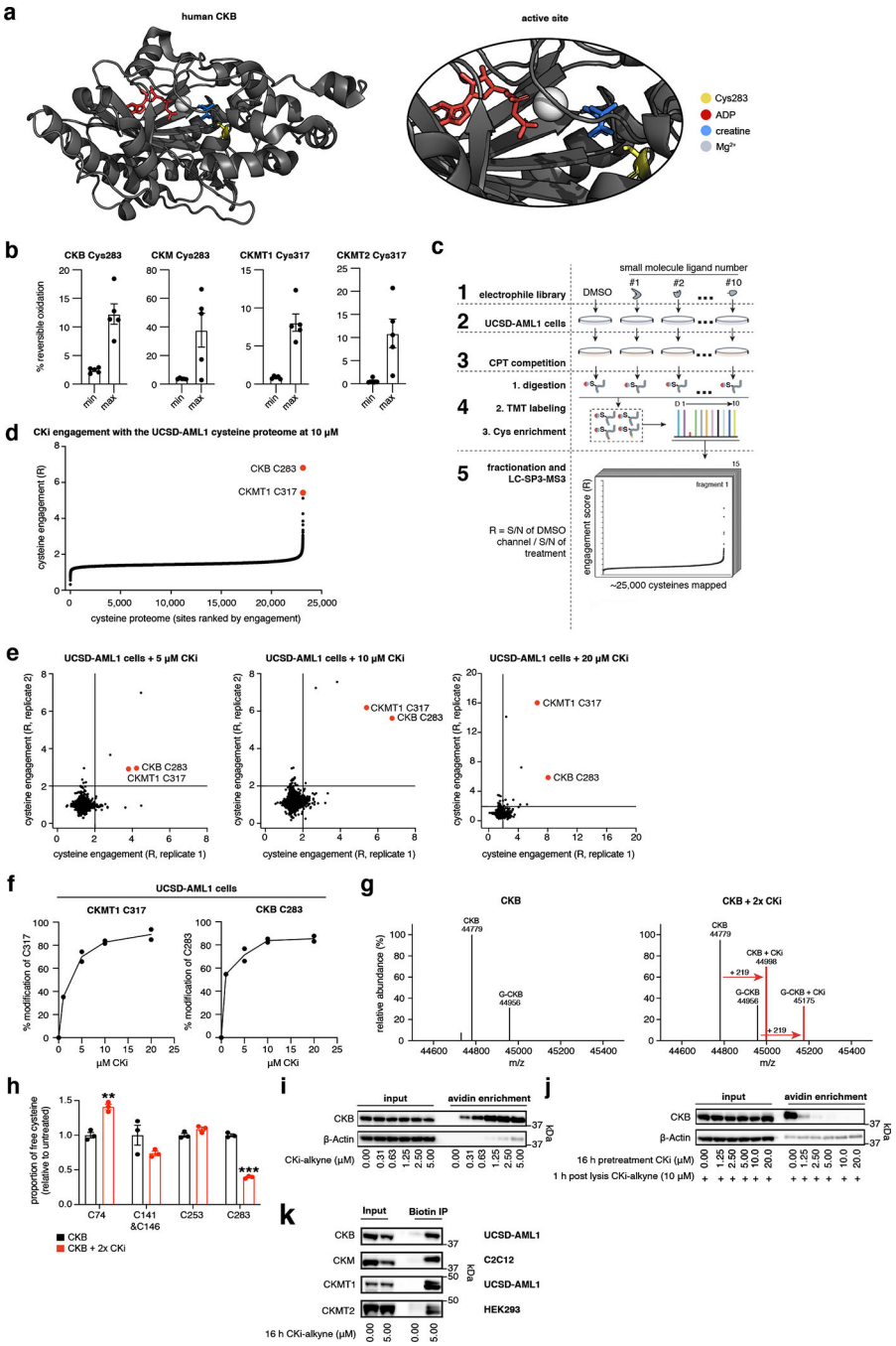

Figure 1: Ultra-deep chemoproteomics identifies a potent and selective small molecule that engages the CK active site cysteine.

(a) Crystal structure of human CKB highlighting Cys283, ADP, creatine, Mg^{2+}. PDB: 3B6R.

(b) Oximouse redox proteomic dataset identifies CKB C283, CKM C283, CKMT1 C317, and CKMT2 C317 as dynamically oxidatively modified across mouse tissues (data from ref. [17]) min and max values report the minimum and maximum observed reversible oxidation modification values from the Oximouse dataset. n=5.

(c) CPT labeling, IMAC enrichment, and MS analysis workflow for identifying cysteine engaged with CKi.

(d) % cysteine engagement (R = S/N DMSO / S/N CKi) determined by CPT enrichment reflects over 70% engagement of CKi for CKB 283 and CKMT1 C317 in a selective manner.
(e) Pairwise comparisons between UCSD-AML1 replicates treated with 5, 10, and 20 μM CKi for 30 min followed by CPT enrichment.
(f) CKMT1 C317 and CKB C283 site specific % modification in UCSD-AML1 across a range of concentrations. n=2 biological cell replicates.
(g) Left: Intact protein MS of 800 nM human recombinant CKB incubated for 2 h with DMSO at 37 °C.
Right: Intact protein MS of 800 nM human recombinant CKB incubated for 2 h with 1.6 μM CKi at 37 °C. G-CKB is α-N-6-phosphogluconoylation modification of His Tag of recombinant CKB.
(h) Quantitative determination of % engagement of cysteines with human recombinant CKB incubated with DMSO or CKi for 2 h at 37 °C via MS. n=3 independent experiments.
(i) Lysates from cells treated with CKi-alkyne subjected to copper-catalyzed cycloaddition reaction with biotin-azide followed by avidin enrichment, and immunoblot for CKB. Representative blot from 3 independent experiments shown.
(j) Pre-treatment of cells with CKi followed by a molar excess of CKi-alkyne prior incubation with biotin-azide followed by avidin enrichment, and immunoblot for CKB. Representative blot from 3 independent experiments shown.
(k) Immunoblot of different CK isoforms in cell types treated with Aki-Alkyne, lysate from cells treated with CKi-alkyne were subjected to copper-catalyzed cycloaddition reaction with biotin-azide followed by avidin enrichment, and immunoblot. Representative blot from 3 independent experiments shown.
Data are presented as average ± s.e.m. *$p < 0.05$, **$p < 0.01$, ***$p < 0.001$ (two-tailed Student’s t test for pairwise comparisons, one-way ANOVA for multiple comparisons involving one independent variable).

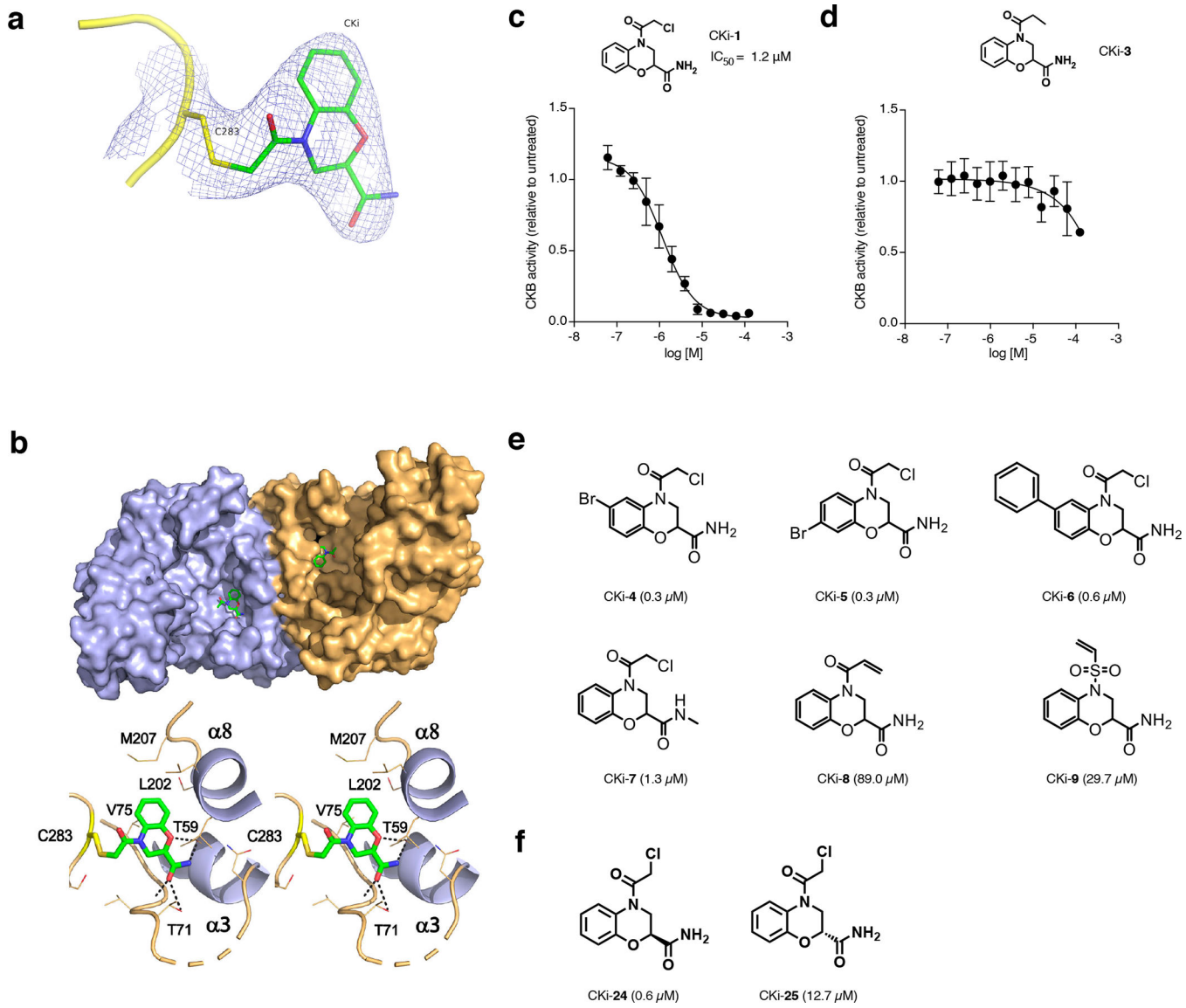

Figure 2: Structural basis for CK inhibition by CKi.

(a) Electron density of CKi in the active site of CKB. A 2FO-FC map of CKi and its attached residue (Cys283) at sigma 0.8.

(b) Crystal structure of human CKB in complex with CKi. Surface representation of the homodimer in light blue and light orange and CKi in green stick format (top). A 3D stereoscopic view of the CKi binding site details with secondary structures shown in ribbon format, CKi and Cys283 in green and yellow stick format, respectively; residues within 5Å of CKi are labelled and shown in line format and CKi-mediated hydrogen bonds shown as dashed lines (bottom).

(c) Recombinant CKB phosphotransfer activity ± 2 h preincubation with CKi. n=3.

(d) Recombinant CKB phosphotransfer activity ± 2 h preincubation with reversible on-covalent analog of CKi. n=3.

(e) Structure of select CKi analogs and biochemical IC_{50} for CKB phosphotransfer activity.

(f) Structure of CKi enantiomers and biochemical IC_{50} for CKB phosphotransfer activity.

Data are presented as average ± s.e.m. *p < 0.05, **p < 0.01, ***p < 0.001 (two-tailed Student's t test for pairwise comparisons, one-way ANOVA for multiple comparisons involving one independent variable).

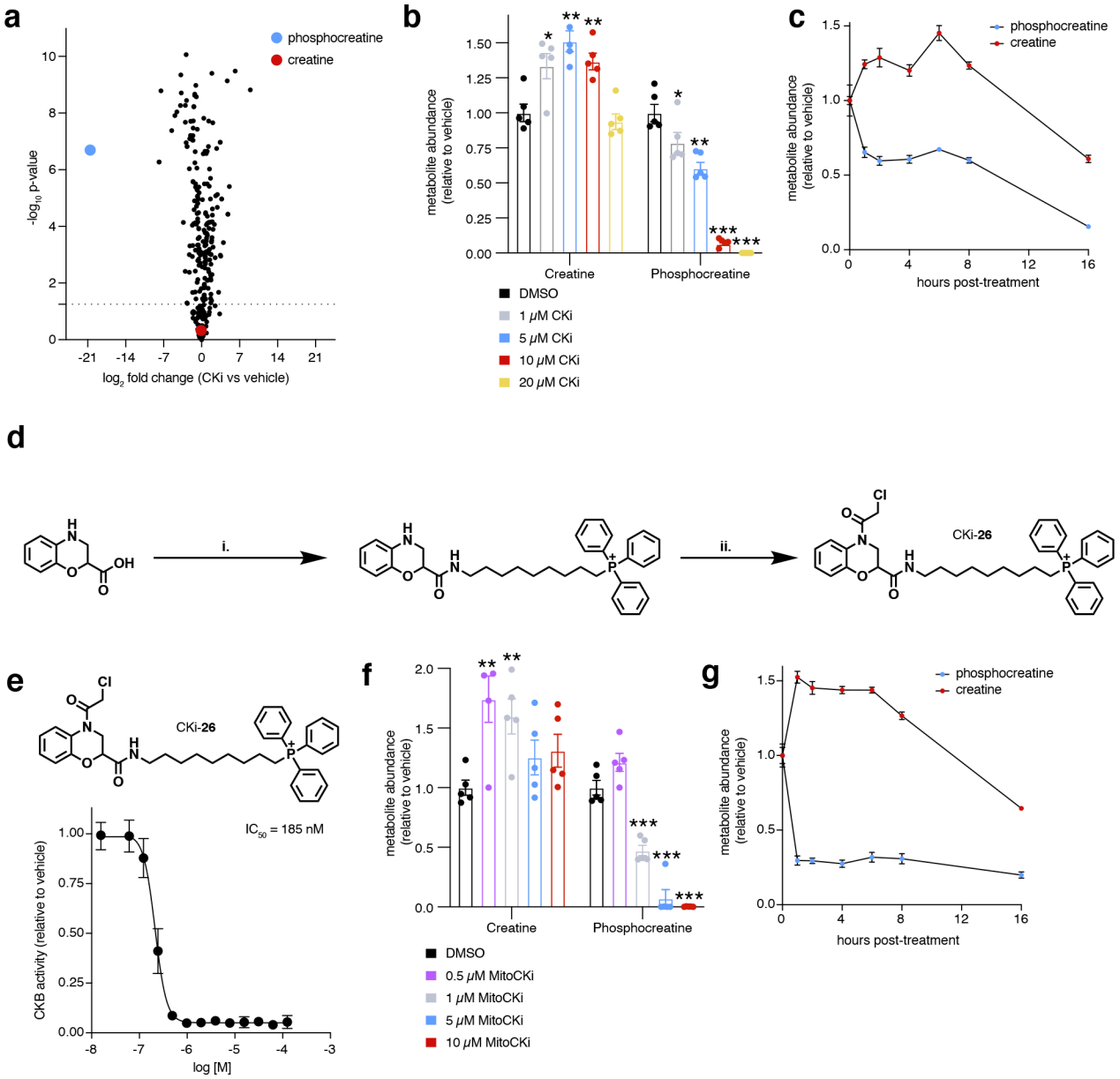

Figure 3: CKi and MitoCKi deplete creatine phosphagen energetics in cells.

(a) Comparative metabolomics analysis to identify metabolite abundance changes in UCSD-AML1 treated with 20 μM CKi for 16 h. n=5.

(b) Creatine and phosphocreatine abundance in UCSD-AML1 cells treated with 0, 1, 5, 10, and 20 μM CKi for 16 h. n=5.

(c) Creatine and phosphocreatine abundance in UCSD-AML1 cells treated with 10 μM CKi over 16 h. n=5.

(d) Synthesis of MitoCKi. See methods for details.

(e) Recombinant CKB phosphotransfer activity ± 2 h preincubation with CKi. n=3.

(f) Creatine and phosphocreatine abundance in UCSD-AML1 cells treated with 0, 1, 5, and 10 μM MitoCKi for 16 h. n=5.

(g) Creatine and phosphocreatine abundance in UCSD-AML1 cells treated with 10 μM MitoCKi over 16 h. n=5.

Data are presented as average ± s.e.m. *p < 0.05, **p < 0.01, ***p < 0.001 (two-tailed Student's t test for pairwise comparisons, one-way ANOVA for multiple comparisons involving one independent variable).

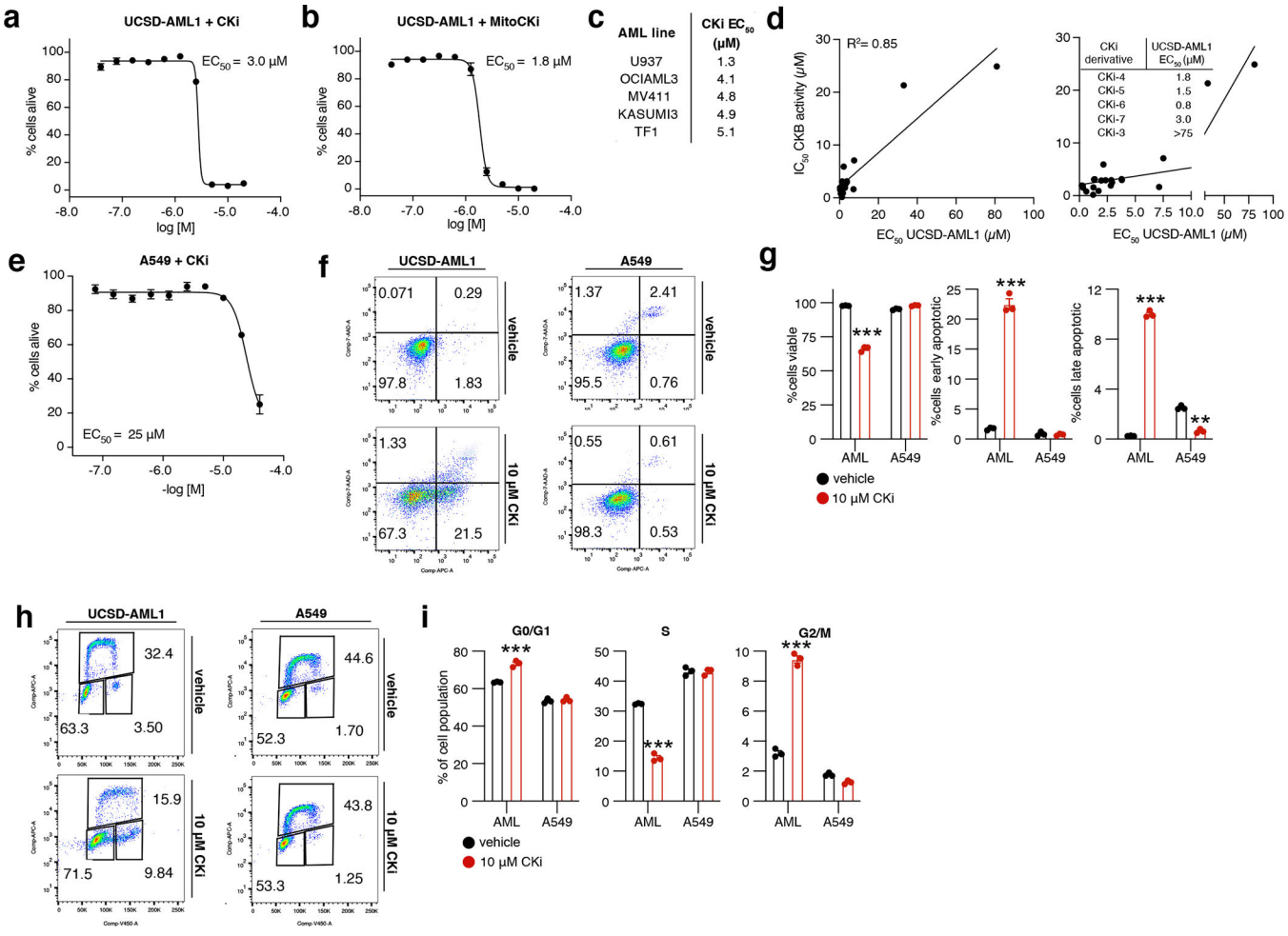

Figure 4: CKi and MitoCKi exploit creatine-energetics dependency in AML to drive cytotoxicity.

(a) The effect of CKi on cell viability in UCSD-AML1 cells. n=8.

(b) The effect of MitoCKi on cell viability in UCSD-AML1 cells. n=8.

(c) The effect of CKi on cell viability in different AML cells. n=8.

(d) (left) Correlation of CKi analog biochemical IC_{50} against recombinant CKB and EC_{50} in UCSD-AML1 cells. (right) Summary of EC_{50} in UCSD-AML1 of improved CKi derivatives described in Figure 2 as well as reversible CKi control.

(e) The effect CKi on cell viability in A549 cells. n=8.

(f) Flow cytometry analysis using Annexin V and 7-AAD staining of UCSD-AML1 or A549 cells treated with DMSO or 10 μM CKi for 16 h.

(g) Quantification of fraction of cells that are apoptotic after 16 h of treatment with 10 μM CKi. n=3

(h) Flow cytometry analysis using Click-iT Plus EdU Alexa Fluor 647 and FxCycle Violet staining of UCSD-AML1 or A549 cells treated with DMSO or 10 μM CKi for 16 h.

(i) Quantification of fraction of cells that are in S, G0/G1 and G2/M phase of the cell cycle after 16 h of treatment with 10 μM CKi. n=3.

Data are presented as average ± s.e.m. *p < 0.05, **p < 0.01, ***p < 0.001 (two-tailed Student's t test for pairwise comparisons, one-way ANOVA for multiple comparisons involving one independent variable).

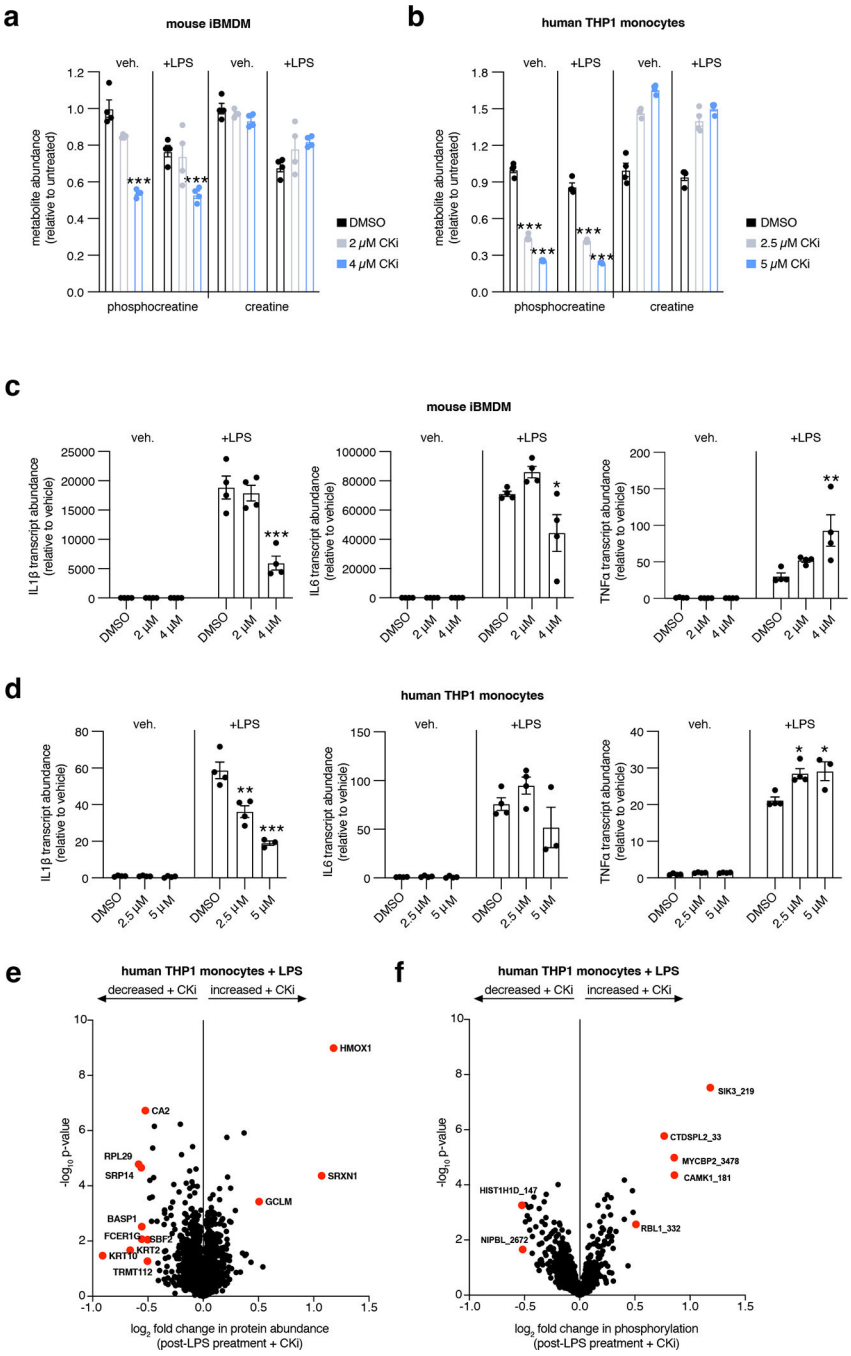

Figure 5: Macrophages and monocytes require the creatine phosphagen system to support pro-inflammatory cytokine production.

(a) Abundance of creatine and phosphocreatine in BMDMs treated with CKi for 2 h with and without LPS. n=5

(b) Abundance of creatine and phosphocreatine in THP1s treated with CKi for 2 h with and without LPS. n=5

(c) Abundance of IL1β, IL6, and TNFα transcripts in BMDMs treated with CKi for 2 h with and without LPS. n=5.

(d) Abundance of IL1β, IL6, and TNFα transcripts in THP1s treated with CKi for 2 h with and without LPS. n=5.

(e) Proteomic analysis of THP1 treated with DMSO or 10 μM CKi for 2 h followed by 100 ng mL^{-1} LPS for 30 min. Proteins upregulated and downregulated by at least a fold change of 0.5 are highlighted in red.

(f) Phopshoproteomic analysis of THP1 treated with DMSO or 10 μM CKi for 2 h followed by 100 ng mL^{-1} LPS for 30 min. Proteins upregulated and downregulated by at least a fold change of 0.5 are highlighted in red.

Data are presented as average ± s.e.m. *$p < 0.05$, **$p < 0.01$, ***$p < 0.001$ (two-tailed Student's t test for pairwise comparisons, one-way ANOVA for multiple comparisons involving one independent variable).